AD_____

Award Number: **W81XWH-13-1-0086**

TITLE: **Circumventing Therapeutic Resistance and the Emergence of Disseminated Breast Cancer Cells Through Non-Invasive Optical Imaging**

PRINCIPAL INVESTIGATOR: **Michael J. Therien**

CONTRACTING ORGANIZATION: **Duke University**
Durham, NC 27705-4677

REPORT DATE: **July 2014**

TYPE OF REPORT: **Annual**

PREPARED FOR: U.S. Army Medical Research and Materiel Command
Fort Detrick, Maryland 21702-5012

REPORT DOCUMENTATION PAGE

Form Approved
OMB No. 0704-0188

1. REPORT DATE	2. REPORT TYPE	3. DATES COVERED
July 2014	Annual	1 July 2013 - 30 June 2014

4. TITLE AND SUBTITLE
Circumventing Therapeutic Resistance and the Emergence of Disseminated Breast Cancer Cells Through Non-Invasive Optical Imaging

5a. CONTRACT NUMBER
W81XWH-13-1-0086

5b. GRANT NUMBER
W81XWH-13-1-0086

5c. PROGRAM ELEMENT NUMBER

6. AUTHOR(S)
Michael J. Therien, Neil L. Spector

E-Mail: michael.therien@duke.edu, neil.spector@duke.edu

5d. PROJECT NUMBER

5e. TASK NUMBER

5f. WORK UNIT NUMBER

7. PERFORMING ORGANIZATION NAME(S) AND ADDRESS(ES)
Duke University
2200 W. Main Street
Durham, NC 27705-4677

8. PERFORMING ORGANIZATION REPORT NUMBER

9. SPONSORING / MONITORING AGENCY NAME(S) AND ADDRESS(ES)
U.S. Army Medical Research and Materiel Command
Fort Detrick, Maryland 21702-5012

10. SPONSOR/MONITOR'S ACRONYM(S)

11. SPONSOR/MONITOR'S REPORT NUMBER(S)

12. DISTRIBUTION / AVAILABILITY STATEMENT
Approved for Public Release; Distribution Unlimited

13. SUPPLEMENTARY NOTES

14. ABSTRACT

Herein we explore a series of optically distinct near infrared emissive polymersomes (NIREPs; biodegradable polymer vesicles that manifest extraordinarily high irradiances and are ideally suited for in vivo optical imaging), each conjugated to different antibodies for the non-invasive molecular imaging of all breast cancer sites within a patient, including micrometastases. In Year 1, we have taken significant steps to optimize NIREP fabrication protocols to ensure immunoreactive antibodies can be reproducibly conjugated to the surface of NIREPs. We have designed and synthesized the most extensive family of PEO-b-PCL copolymers that vary over the largest range of number-average molecular weights (Mn: 3.6 - 57K), PEO weight fractions (fPEO: 0.08 - 0.33), and PEO chain lengths (0.75 – 5.8K) reported to date. With these, we have demonstrated using comparative morphology diagrams, that a multiplicity of PEO-b-PCL diblock copolymer compositions are able to give rise to nanoscale vesicles. The broad range of polymersome-forming PEO-b-PCL compositions suggest the ability to construct extensive families of nanoscale vesicles of varied bilayer thickness, providing the ability to tune the timescales of vesicle degradation in vivo. Lastly, we have established four pairs of parental and isogenic matched tamoxifen (tam)-resistant cell lines (MCF7, T47D, MDA-MB-361 and HCC1428), and characterized the changes in cell surface protein expression that occurs with onset of resistance. We have found that members of the HER receptor family (EGFR/HER1; HER2; HER3) are upregulated with the development of tam-resistance; furthermore, differences in receptor expression between ER+ cell lines have been characterized. These reagents are critical for evaluation of the selectivity of a panel of antibody-conjugated NIREPs.

15. SUBJECT TERMS
Breast cancer, emissive polymersomes, near infrared fluorescence, therapeutic resistance, molecular profiling, personalized medicine, imaging, active targeting

16. SECURITY CLASSIFICATION OF:			17. LIMITATION OF ABSTRACT	18. NUMBER OF PAGES	19a. NAME OF RESPONSIBLE PERSON
a. REPORT	b. ABSTRACT	c. THIS PAGE			USAMRMC
U	U	U	UU	27	19b. TELEPHONE NUMBER *(include area code)*

Table of Contents

Introduction

Breast cancer (BC) is a molecularly heterogeneous disease, which can be categorized into subtypes based on the tumor biology.[1,2] HER2 over-expressing cancers (HER2+) for example, account for 25–30% of diagnosed BCs and are associated with early metastasis and poor survival prognosis.[3] Treatments for HER2+ BCs, such as Herceptin,[4] directly target the HER2 cell membrane receptor.[5] Such treatments are specific to HER2+ BCs, with no effect on other tumor subtypes e.g. estrogen receptor overexpressing cancers (ER+, luminal A subtype). Similarly, ER+ BC are treated with endocrine therapies targeting either ER directly e.g. tamoxifen,[6] or production of the receptor ligand (estradiol) e.g. aromatase inhibitors.[7,8] It is therefore crucial to molecularly profile a cancer to prescribe the correct program of treatment. Diagnosis and subsequent treatment of BC is often based on analysis of a single biopsy of a primary tumor, and the surrounding lymph nodes. However, this method is flawed in advanced stage cancers, as the molecular profile of the cancer may differ at metastatic sites and/or between metastases in different organs.[9] Furthermore, most advanced stage breast cancers that initially respond to targeted therapy, whether HER2+ or ER+, become resistant to treatment, generally in less than 12 months, resulting in disease progression.[10,11] The molecular heterogeneity of BC tumors, coupled with the diverse mechanisms and dynamic nature of therapy resistance,[12–18] illustrate that this method of diagnosis is insufficient to predict a tumor's response to treatment. This accounts for the mixed clinical responses to treatment observed in advanced stage BC patients, where some sites regress while others see progression. Developing effective treatment strategies for BC requires the ability to identify the molecular subtypes of each tumor site, and understand the mechanisms involved in the development of therapeutic resistance. However, biopsying each site multiple times over the course of treatment is impossible. We proposed that near-infrared emissive polymersomes (NIREPs), a brightly emissive nanostructure, can be targeted to signature cell surface proteins to enable quantitative, non-invasive optical imaging of molecularly heterogeneous sites of BC in vivo. In this DoD 2013-2014 annual report, we provide an update on our progress to develop antibody-conjugated NIREPs capable of distinguishing between phenotypically distinct BC cells.

Body

Aim 1 (Years 1–3): Profile a panel of molecularly heterogeneous human breast cancer cell lines using cocktails of antibody-conjugated NIREPs.

Therien Group: In our prior work, we demonstrated that NIREPs featuring surfaces functionalized with the humanized anti-HER2 monoclonal antibody trastuzumab (Herceptin), were able to discriminate between HER2+ and HER2– cell lines in *in vitro* experiments (Figure 1d). The intent of this project is to extend these studies by developing a series of other antibody-conjugated NIREPs, each targeting a specific breast cancer-relevant cell surface antigen. Each unique NIREP would contain a porphyrin oligomer fluorophore to enable wavelength-based detection of cell receptor type (Figure 1a–c).

In a separate DOD project (PI: Armstrong) it was found that NIREPs bearing antibodies targeted to EPCAM saw batch-to-batch variability in flow cytometry experiments for binding to EPCAM over-expressing cells. Investigation of new batches of anti-HER2-NIREPs found similar difficulties in reproducibility (**Figure 2**). In some batches, high uptake of up to 85,000 NIREPs per HER2+ SKBR3 cell were observed; in others, uptake levels matched that of control NIREPs conjugated to an isotype-matched IgG antibody. This prompted us to reinvestigate our protocols in detail. Our previously used bicinchoninic assay (BCA) used to determine the degree of antibody functionalization on the surface on the NIREP was unable to distinguish between covalently bound-antibody and surface associated antibody. Therefore, the use of this assay to determine the efficiency of different antibody-coupling chemistries in some cases may have yielded inaccurate data.

We have therefore invested time optimizing our coupling protocols and characterization methods as described below.

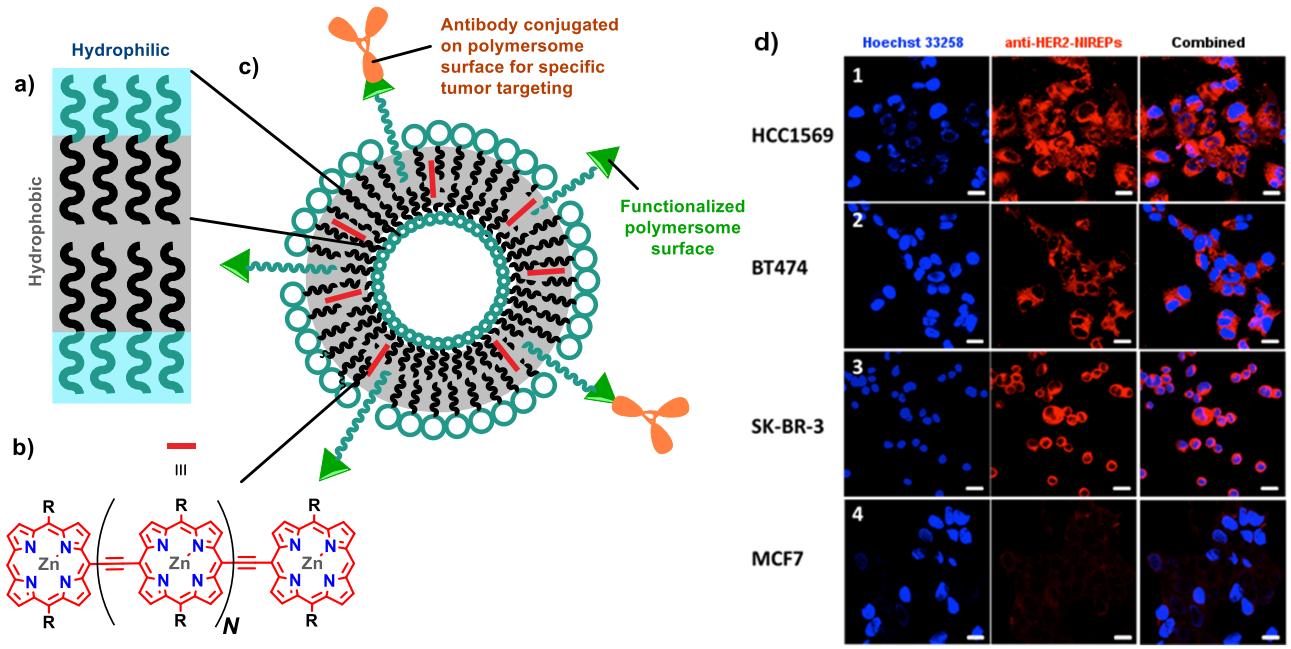

Figure 1 Schematic depiction of an antibody-conjugated NIREP: a) Polymersomes consist of a bilayer of amphiphiles which self-assemble in aqueous conditions. The resulting vesicle has the hydrophilic head groups pointing into the interior of the vesicle, and towards bulk solvent, with the hydrophobic chains sequestered within the membrane; b) The lipophilic membrane can be loaded with near-IR fluorophores (PZn_N compounds, e.g. PZn_3: λ_{ex} = 786 nm; λ_{em} = 809 nm). Number of porphyrins *N* and solubilizing groups R can be varied to alter emission wavelength; c) Antibody-conjugated NIREPs enable tumor specific cell targeting. (d) Anti-HER2 NIREPs can discriminate between HER2+ cells (HCC1569, BT474 and SKBR3 cells) and HER2 negative cells (MCF7). Left column: nuclei stained with Hoechst 33258 (λ_{em} = 461 nm). Center column: PZn_3 anti-HER2-NIREPs (λ_{em} = 809 nm) located on the membrane surface and in the cell cytoplasm. Right column: Overlay of the micrographs from the blue and red channels.

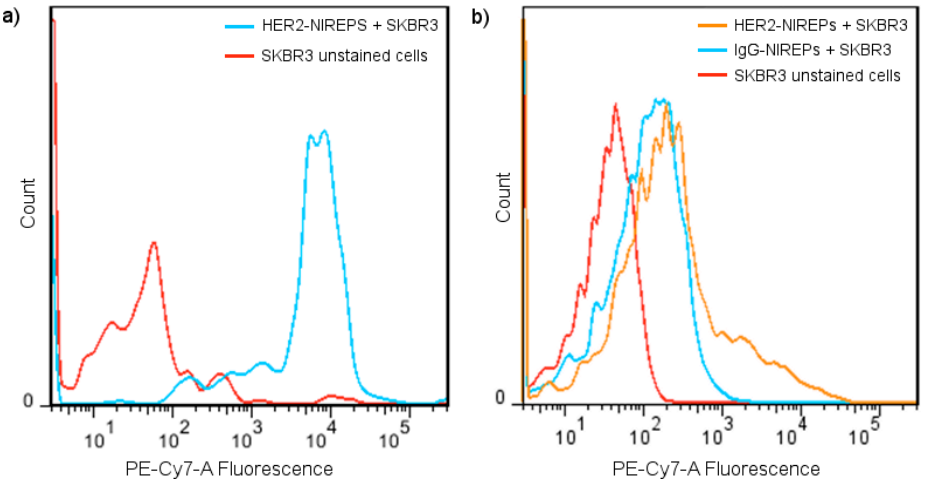

Figure 2 Flow sorting of HER2+ SKBR3 cells using anti-HER2-NIREPs; detection using the Cy7 channel (>790 nm near infrared wavelength). **a)** Batch 1: Large uptake of anti-HER2-NIREPs into SKBR3 cells gives a large increase in fluorescence compared to unstained cells; **b)** Batch 2: Negligible uptake of anti-HER2-NIREPs into SKBR3 cells, with very similar levels of fluorescence to cells incubated with control IgG-conjugated NIREPs.

Conjugation chemistries

We have reexplored two orthogonal conjugation methods for the coupling of antibodies to the surface of NIREPs. The first method utilizes a fluoronitrobenzoic acid (FNB) functionality which is introduced onto the block-copolymer end hydroxyl group in a single, high yielding step (Scheme 1).[19]

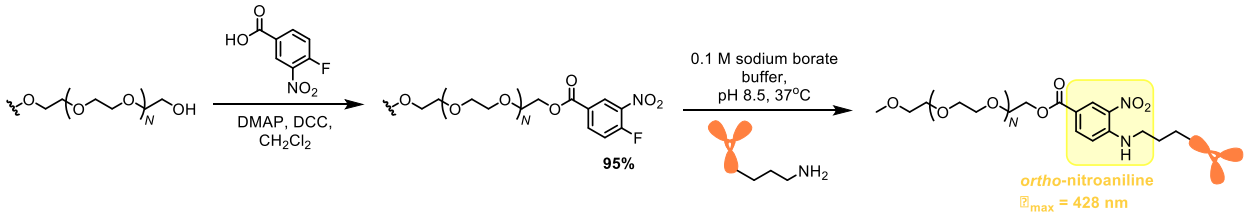

Scheme 1 Functionalization of PDB-*b*-PEO diblock copolymer OB18 with FNB. Conjugation of a bioligand *via* a lysine residue yields a chromophoric *ortho*-nitroaniline linker highlighted in yellow.

The advantage of this method is twofold. Firstly, FNB is reactive to primary amines, which in the case of antibodies, is readily available *via* the protein N-terminus or surface lysine residues. The abundance of these residues in antibodies means prior chemical modification of antibodies is unnecessary, minimizing the possibility of antibody-deactivation through inadvertent modification of the complementarity determining regions (CDR). Secondly, conjugation of primary amines to the *para*-position of FNB yields a chromophoric *ortho*-nitroaniline, which absorbs strongly at 428 nm. This provides an internal 'reporter' that enables us to quantify covalently bound antibody using absorption at this wavelength. Our group has previously used FNB-based chemistry to successfully functionalize NIREPs with the cell-penetrating Tat peptide for tracking dendritic cells in vivo,[20,21] so we are confident we can adapt this protocol for the attachment of antibodies.

The second method we are exploring uses a sulfosuccinimidyl-4-(*N*-maleimidomethyl)cyclohexane-1-carboxylate (sulfo-SMCC) linker, which we can use to couple antibodies to the NIREP surface *via* a sulfhydryl group (Scheme 2).

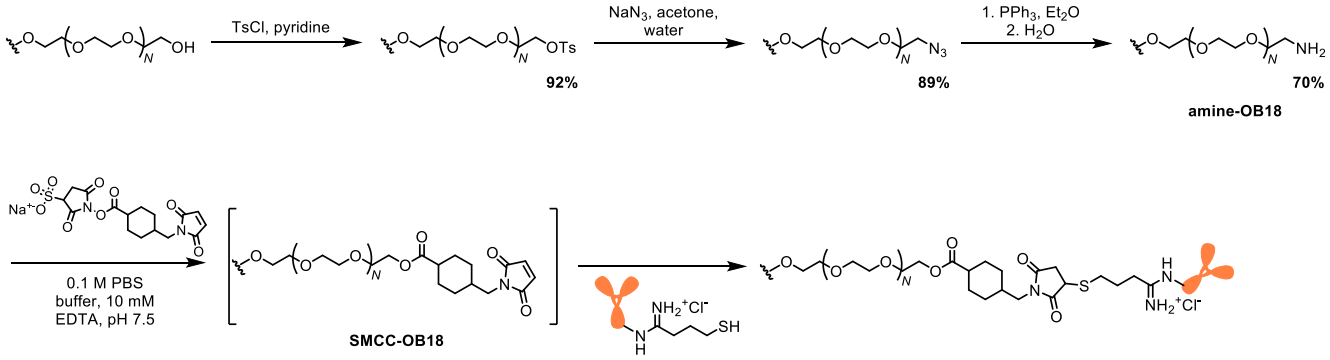

Scheme 2 Synthesis of SMCC-functionalized PEO-*b*-PBD co-polymer OB18. SMCC-OB18 reacts with a thiol group introduced onto an antibody using 2-iminothiolane (Traut's reagent).

Sulfhydryl functionality can be introduced onto the surface of antibodies by modification of native lysines with 2-iminothiolane (Traut's reagent), without destruction of antibody immunoreactivity. Many examples of sulfo-SMCC being used as a protein-drug conjugate linker exist in the literature, most notably in the case of the 2013 FDA-approved chemotherapy drug ado-trastuzumab emtansine (Kadcyla®),where Herceptin is ligated through sulfo-SMCC to the cytotoxic agent mertansine (DM1).[22] We will evaluate the conjugation efficiency of antibodies to sulfo-SMCC functionalized NIREPs using size exclusion chromotography and SDS-PAGE.

NIREP construction

Using our newly validated functionalized OB18 polymer, we can construct NIREPs using our well-established methodology (Figure 3).

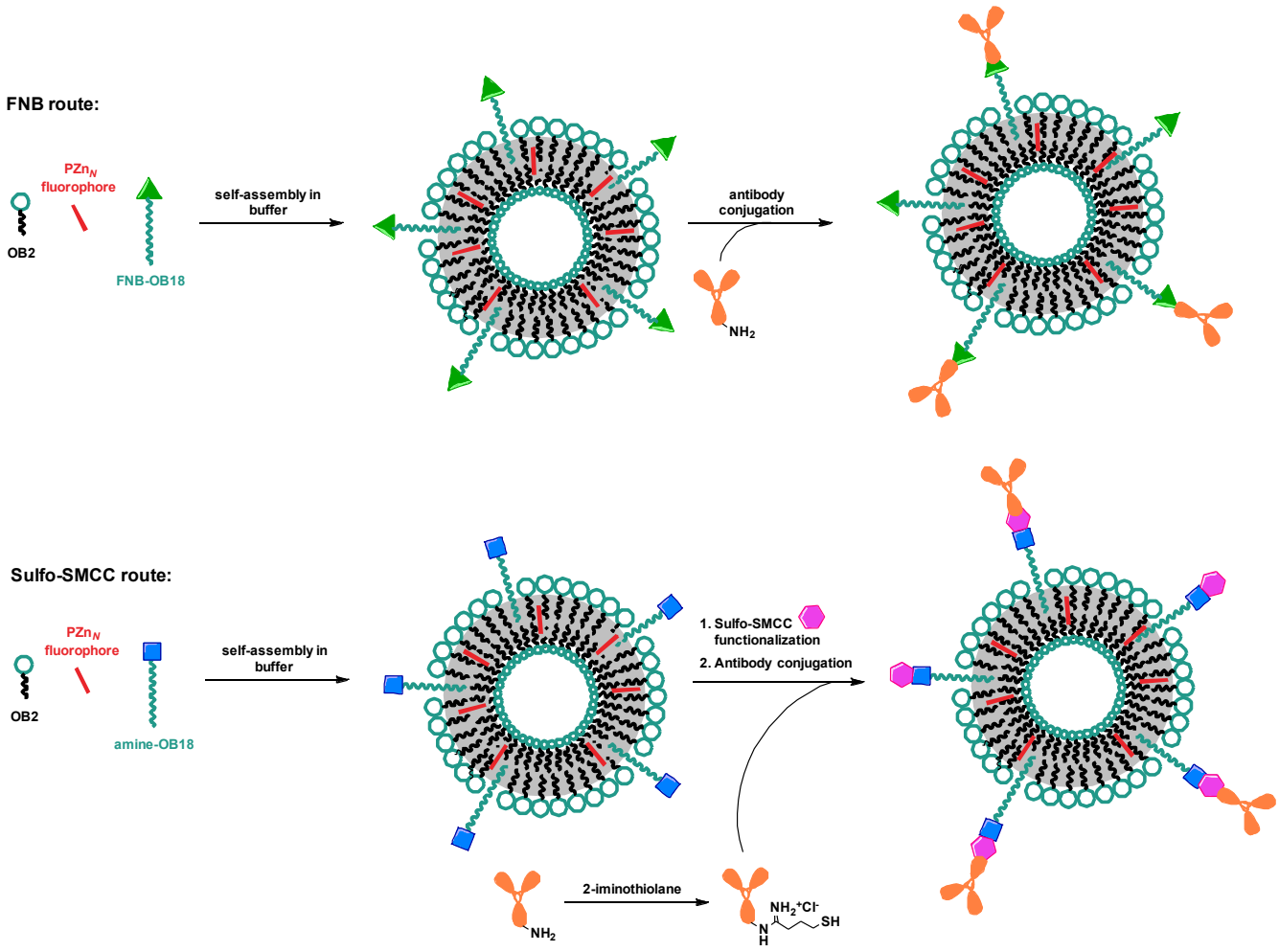

Figure 3 Construction of antibody-conjugated NIREPs via FNB- and sulfo-SMCC routes.

FNB/amine functionalized PEO(3600)-*b*-PBD(6800) diblock copolymer (OB18) was mixed with PEO(1300)-*b*-PBD(2500) diblock copolymer (OB2) in a 5:95 molar ratio. The mixed diblock co-polymer and porphyrin fluorophore (PZn_N) were dissolved in dichloromethane in a 40:1 polymer:fluorophore molar ratio. The solution was plated onto a roughened Teflon film and dried under vacuum overnight. Polymersomes were formed upon the addition of aqueous buffer (for FNB: 0.1 M sodium borate buffer, pH 8.5; for amine-OB18: 0.1 M PBS buffer, pH 7.5) and sonication for 1 h. A narrow size distribution of nano-size polymersomes was achieved with serial extrusion using a Liposofast Basic handheld extruder equipped with 400-, 200- and 100 nm polycarbonate membranes (Avestin Inc., Ottawa, Ontario). The resulting polymersomes are characterized by dynamic light scattering (DLS) and confocal microscopy.

To avoid maleimide deactivation by hydrolysis under aqueous conditions, SMCC-activated NIREPs are assembled using the precursor amine-OB18. The amine-NIREP can subsequently be treated with sulfo-SMCC, rapidly purified on a desalting column to remove excess linker, and then incubated with thiolated antibody. The presence of the cyclohexane ring in sulfo-SMCC confers significantly greater stability under aqueous conditions than our previously used *m*-maleimidobenzoyl-N-hydrosuccinimide ester (MBS) linker,[23] which will improve conjugation efficiencies of the antibody to the NIREP surface.

Antibody modification

Chemical modification of an antibody has the potential to adversely affect its immunoreactivity. Trastuzumab contains between 80–95 lysine residues which potentially can act as a chemical handle either for direct attachment to FNB-NIREPs, or for conversion to a SMCC-reactive thiol group. We will explore the effects of antibody functionalization in the following experiments:

1. Thiolation. We will assay the number of thiol groups introduced by 2-iminothiolane onto the surface of the antibody using Elmann's reagent. Reaction conditions (temperature, reaction time and reagent concentrations) will be altered accordingly to minimize the number of thiol groups introduced.
2. Coupling reactions. Trastuzumab will be conjugated to triethylene glycol (TEG) models as shown in Scheme 3. The immunoreactivity of the resulting conjugates will be evaluated using flow cytometry with HER2+ BC cells, and ELISA. If appropriate, different coupling conditions (temperature, buffer, reaction times, concentrations) will be explored.

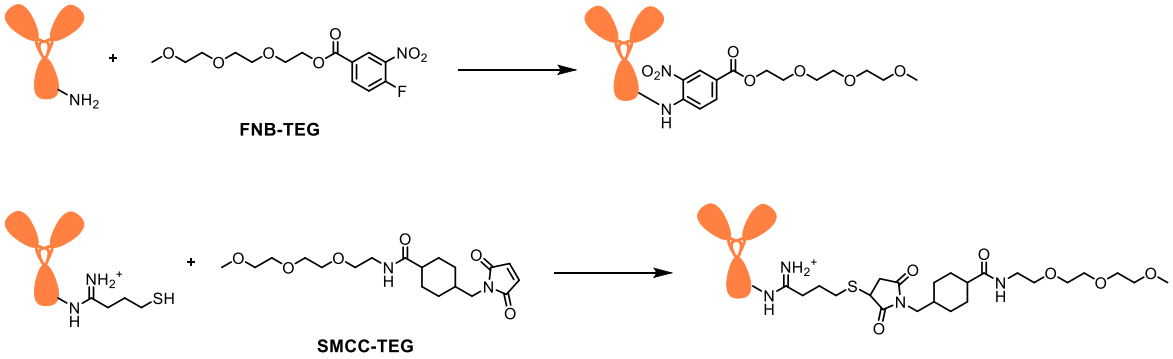

Scheme 3 Reaction of antibodies with functionalized triethylene glycol (TEG) models to evaluate the effect of covalent modification on immunoreactivity.

Aim 1a (Year 1): Cell Lines

Spector Group: Our *hypothesis* is that a cocktail of optically distinct near infrared NIREPs (soft matter, biodegradable, NIR emissive nanoscale vesicles that manifest extraordinarily high irradiances and are ideally suited for *in vivo* optical imaging), each conjugated to different antibodies that target one of multiple therapeutically relevant cell surface proteins expressed on breast cancer cells, can provide non-invasive molecular images of the active BC sites within a patient, including micrometastases. A NIREP-based imaging approach could then be used to select appropriate combinations of targeted therapies taking into account the molecular heterogeneity that exists in a patient.

Furthermore, NIREP-based *in vivo* optical imaging will enable spatial and temporal characterization of the effects of targeted therapies on the molecular profile of tumors, some of which have been shown to contribute to the development of therapeutic auto-resistance. To test our hypothesis, particularly the second aspect having to do with characterizing the molecular changes associated with therapeutic resistance to targeted therapies, we must first develop isogenic matched HER2+ human breast cancer cell lines, parental and cell counterparts that have become resistant to targeted therapies used in breast cancer treatment. As provided in the original grant application, we have developed lapatinib resistant HER2+ human breast cancer cell lines and characterized

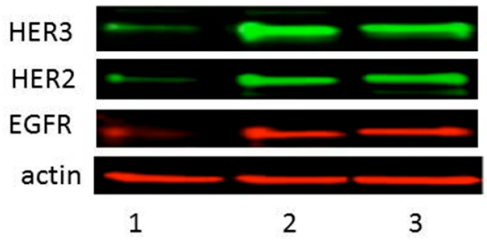

Figure 4 Increased HER receptor expression in response to tam-treated MDA-MB-361 cells and tam-resistant 361 cells. Steady-state levels of the indicated proteins in control 361 cells treated with vehicle (0.01% DMSO) alone (lane 1); parental 361 cells treated with 1 μM tamoxifen for 72 hrs (lane 2); and tamoxifen-resistant 361 cells cultured in the continuous presence of 1 μM tamoxifen. Actin steady-state protein levels served as controls for equal loading of protein.

differences between the lapatinib-sensitive parental and resistant cell counterparts.[12,15] For example, lapatinib-resistant SKBR3 cells (rSKBR3) preferentially express the stem cell antigen CD146 compared with isogenic matched parental cells. CD146 is one of the targets for our antibody-conjugated NIREP based imaging approach. During the past year we sought to expand our repertoire of isogenic matched parental and targeted therapy resistant breast cancer cell lines to include ER+ tumors. We have established several tamoxifen (tam) resistant ER+ human breast cancer cell lines by continuously exposing parental cells to clinically relevant concentrations of tamoxifen. Establishing stable tam-resistant cell lines turned out to be a challenging and protracted process that took months. We now have four pairs of parental and matched tam-resistant cell lines (MCF7; T47D; MDA-MB-361; HCC1428).

We have found that protein expression in members of the HER receptor family (EGFR/HER1; HER2; HER3) is up-regulated with the development of tam-resistance (Figure 4). Even acute treatment of parental MDA-MB-361 cells led to an increase in HER receptor expression. We can now use antibody-conjugated NIREPs targeting EGFR, HER2, and HER3 to distinguish parental from tam-resistant cell counterparts. In contrast, we see a different effect of tam-resistance on HER receptor expression in ER+ MCF7 and T47D human breast cancer cell lines (Figure 5). In MCF7 cells, expression of EGFR is increased while expression of HER2 and HER3 decreased in tam-resistant cells compared with parental cell counterparts. Similarly, HER2 and HER3 expression are decreased with the development of tam-resistance in T47D. We expect to characterize these changes using specific antibodies to HER receptors conjugated to NIREPs.

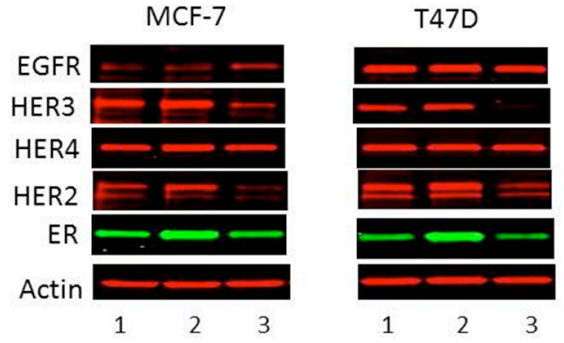

Figure 5 Changes in HER receptor expression with development of tam-resistance. Steady-state levels of the indicated proteins in control MCF7 and T47D cells treated with vehicle (0.01% DMSO) alone (lane 1); parental cells treated with 1 μM tamoxifen for 72 hrs (lane 2); and tamoxifen-resistant cells cultured in the continuous presence of 1 μM tamoxifen. Actin steady-state protein levels served as controls for equal loading of protein.

Key Research Accomplishments

- Synthesis of nanosized bioresorbable NIREPs for *in vivo* applications

Nanoparticles formed from diblock copolymers of FDA-approved PEO and PCL have generated considerable interest as *in vivo* drug delivery vehicles. We designed and synthesized the most extensive family of PEO-*b*-PCL copolymers that vary over the largest range of number-average molecular weights (M_n: 3.6 - 57K), PEO weight fractions (f_{PEO}: 0.08 - 0.33), and PEO chain lengths (0.75 – 5.8K) reported to date.[24] These polymers were synthesized in order to establish the full range of aqueous phase behaviours of these diblock copolymers and to specifically identify formulations that were able to generate bilayered polymersomes. Cryogenic transmission electron microscopy (cryo-TEM) was utilized in order to visualize the morphology of these structures upon aqueous self-assembly of dry polymer films. Nanoscale polymersomes were formed from PEO-*b*-PCL copolymers over a wide range of PEO weight fractions (f_{PEO}: 0.14 – 0.27) and PEO molecular weights (0.75 – 3.8K) after extrusion of aqueous suspensions. Comparative morphology diagrams, which describe the nature of self-assembled structures as a function of diblock copolymer molecular weight and PEO weight fraction, show that in contrast to micron-scale polymersomes, which form only from a limited range of PEO-*b*-PCL diblock copolymer compositions, a multiplicity of PEO-*b*-PCL diblock copolymer compositions are able to give rise to nanoscale vesicles. These data underscore that PEO-*b*-PCL compositions that spontaneously form micron-sized polymersomes, as well as those that have previously been reported to form polymersomes via a co-solvent fabrication system, provide only

limited insights into the distribution of PEO-*b*-PCL diblocks that give rise to nanoscale vesicles. The broad range of polymersome-forming PEO-*b*-PCL compositions suggest the ability to construct extensive families of nanoscale vesicles of varied bilayer thickness, providing the ability to tune the timescales of vesicle degradation and encapsulant release based on the intended *in vivo* application. Furthermore, these bioresorbable polymersome-forming PEO-*b*-PCL compositions provide important building blocks necessary for the construction of NIREPs suitable for the non-invasive optical imaging of molecularly heterogeneous sites of BC *in vivo*.

- Development of stable tamoxifen (tam) resistant ER+ human breast cancer cell lines for the characterization of targeted therapy resistance using NIREPs.

We have established a panel of parental and isogenic matched human breast cancer cell lines that developed resistance to different targeted therapies used in the treatment of HER2+ and ER+ breast cancers. These reagents are critical to successful achievement of our goals. They provide a molecularly diverse set of tumor cell lines to evaluate the selectivity of a panel of antibody-conjugated NIREPs. They also provide insight into the molecular changes that are associated with the development of therapeutic resistance to HER2 and ER-targeted therapies, which we propose can be temporally and spatially detected during the course of therapy using antibody-conjugated NIREPs. When the antibody-conjugated NIREPs are generated as described above, we will evaluate their selectivity against these panels of parental and resistant cell lines. In year 2, we will establish luciferase-tagged breast cancer cell lines from the panels described above in preparation for the *in vivo* tumor xenograft studies (Aim 2) proposed for years 2 and 3.

Reportable Outcomes

Publication:

Aqueous Self-Assembly of Poly(ethylene oxide)-block-Poly(ε-caprolactone) (PEO-b-PCL) Copolymers: Disparate Diblock Copolymer Compositions Give Rise to Nano- and Meso-Scale Bilayered Vesicles, W. Qi, P. P. Ghoroghchian, G. Li, D. A. Hammer, and M. J. Therien, *Nanoscale*, **2013**, 5, 10908−10915.

Degrees:

Zhou, R. Engineering Targeted Near Infrared Emissive Polymersomes for Imaging Applications. M.S. Thesis, Duke University, Durham, NC, June 2014.

Cell Lines:

Parental and matched tam-resistant cell lines MCF7, T47D, MDA-MB-361, HCC1428.

Conclusion

While experimental setbacks we have experienced in the first year of our Department of Defense funding have delayed us in achieving the expected outcomes outlined in our Statement of Work, significant steps have been taken to optimize NIREP fabrication protocols. By ensuring that we can reproducibly conjugate immunoreactive antibodies to the surface of NIREPs, we can apply this methodology to rapidly fabricate a series of antibody-conjugated NIREPs for in vivo profiling of molecularly heterogeneous breast cancers. Furthermore, this novel methodology itself will be useful to the wider scientific community. Our expectation is that upon optimizing our coupling procedures, we will quickly progress to a series of antibody-conjugated NIREPs for in vitro testing in Year 2. Our preliminary data with positive batches of anti-HER2-NIREPs demonstrate that NIREPs are a powerful

tool for optically distinguishing between BC tumor subtypes in vitro. The ability of antibody-conjugated NIREPs to simultaneously profile multiple cell antigens of interest in vitro would make them a valuable pre-clinical tool for studying the numerous mechanisms of therapeutic resistance. Our studies have further shown that unfunctionalized NIREPs concentrate at tumor sites owing to their nanometer-sized dimensions. This, coupled with their unprecedented brightness, gives NIREPs the potential to profile of all sites of metastatic disease in vivo for the first time. This would be transformative in the treatment of advanced stage breast cancer, as it would enable a personalized course of treatment to be determined based on an individual's tumor profile. In addition, the ability to characterize mechanisms of therapy resistance in vivo using NIREPs would drastically improve patient survival and remission rates by enabling prompt intervention, and allowing new treatment strategies to be developed.

References

(1) Perou, C. M.; Sørlie, T.; Eisen, M. B.; Rijn, M. van de; Jeffrey, S. S.; Rees, C. A.; Pollack, J. R.; Ross, D. T.; Johnsen, H.; Akslen, L. A.; et al. Molecular Portraits of Human Breast Tumours. *Nature* **2000**, *406*, 747–752.

(2) Sørlie, T.; Perou, C. M.; Tibshirani, R.; Aas, T.; Geisler, S.; Johnsen, H.; Hastie, T.; Eisen, M. B.; Rijn, M. van de; Jeffrey, S. S.; et al. Gene Expression Patterns of Breast Carcinomas Distinguish Tumor Subclasses with Clinical Implications. *Proc. Natl. Acad. Sci.* **2001**, *98*, 10869–10874.

(3) Slamon, D. J.; Clark, G. M.; Wong, S. G.; Levin, W. J.; Ullrich, A.; McGuire, W. L. Human Breast Cancer: Correlation of Relapse and Survival with Amplification of the HER-2/neu Oncogene. *Science* **1987**, *235*, 177–182.

(4) Slamon, D. J.; Leyland-Jones, B.; Shak, S.; Fuchs, H.; Paton, V.; Bajamonde, A.; Fleming, T.; Eiermann, W.; Wolter, J.; Pegram, M.; et al. Use of Chemotherapy plus a Monoclonal Antibody against HER2 for Metastatic Breast Cancer That Overexpresses HER2. *N. Engl. J. Med.* **2001**, *344*, 783–792.

(5) Hynes, N. E.; Lane, H. A. ERBB Receptors and Cancer: The Complexity of Targeted Inhibitors. *Nat. Rev. Cancer* **2005**, *5*, 341–354.

(6) Early Breast Cancer Trialists' Collaborative Group (EBCTCG). Relevance of Breast Cancer Hormone Receptors and Other Factors to the Efficacy of Adjuvant Tamoxifen: Patient-Level Meta-Analysis of Randomised Trials. *The Lancet* **2011**, *378*, 771–784.

(7) Nabholtz, J.-M.; Mouret-Reynier, M.-A.; Durando, X.; Van Praagh, I.; Al-Sukhun, S.; Ferriere, J.-P.; Chollet, P. Comparative Review of Anastrozole, Letrozole and Exemestane in the Management of Early Breast Cancer. *Expert Opin. Pharmacother.* **2009**, *10*, 1435–1447.

(8) Dowsett, M.; Cuzick, J.; Ingle, J.; Coates, A.; Forbes, J.; Bliss, J.; Buyse, M.; Baum, M.; Buzdar, A.; Colleoni, M.; et al. Meta-Analysis of Breast Cancer Outcomes in Adjuvant Trials of Aromatase Inhibitors Versus Tamoxifen. *J. Clin. Oncol.* **2010**, *28*, 509–518.

(9) Lower, E. E.; Glass, E.; Blau, R.; Harman, S. HER-2/neu Expression in Primary and Metastatic Breast Cancer. *Breast Cancer Res Treat* **2009**, *113*, 301–306.

(10) Valabrega, G.; Montemurro, F.; Aglietta, M. Trastuzumab: Mechanism of Action, Resistance and Future Perspectives in HER2-Overexpressing Breast Cancer. *Ann. Oncol.* **2007**, *18*, 977–984.

(11) Osborne, C. K.; Schiff, R. Mechanisms of Endocrine Resistance in Breast Cancer. *Annu. Rev. Med.* **2011**, *62*, 233–247.

(12) Xia, W.; Bacus, S.; Hegde, P.; Husain, I.; Strum, J.; Liu, L.; Paulazzo, G.; Lyass, L.; Trusk, P.; Hill, J.; et al. A Model of Acquired Autoresistance to a Potent ErbB2 Tyrosine Kinase Inhibitor and a Therapeutic Strategy to Prevent Its Onset in Breast Cancer. *Proc. Natl. Acad. Sci.* **2006**, *103*, 7795–7800.

(13) Xia, W.; Liu, Z.; Zong, R.; Liu, L.; Zhao, S.; Bacus, S. S.; Mao, Y.; He, J.; Wulfkuhle, J. D.; Petricoin, E. F.; et al. Truncated ErbB2 Expressed in Tumor Cell Nuclei Contributes to Acquired Therapeutic Resistance to ErbB2 Kinase Inhibitors. *Mol. Cancer Ther.* **2011**, *10*, 1367–1374.

(14) Eichhorn, P. J. A.; Gili, M.; Scaltriti, M.; Serra, V.; Guzman, M.; Nijkamp, W.; Beijersbergen, R. L.; Valero, V.; Seoane, J.; Bernards, R.; et al. Phosphatidylinositol 3-Kinase Hyperactivation Results in Lapatinib Resistance That Is Reversed by the mTOR/Phosphatidylinositol 3-Kinase Inhibitor NVP-BEZ235. *Cancer Res.* **2008**, *68*, 9221–9230.
(15) Rexer, B. N.; Ham, A.-J. L.; Rinehart, C.; Hill, S.; de Matos Granja-Ingram, N.; González-Angulo, A. M.; Mills, G. B.; Dave, B.; Chang, J. C.; Liebler, D. C.; et al. Phosphoproteomic Mass Spectrometry Profiling Links Src Family Kinases to Escape from HER2 Tyrosine Kinase Inhibition. *Oncogene* **2011**, *30*, 4163–4174.
(16) Garrett, J. T.; Olivares, M. G.; Rinehart, C.; Granja-Ingram, N. D.; Sanchez, V.; Chakrabarty, A.; Dave, B.; Cook, R. S.; Pao, W.; McKinely, E.; et al. Transcriptional and Posttranslational up-Regulation of HER3 (ErbB3) Compensates for Inhibition of the HER2 Tyrosine Kinase. *Proc. Natl. Acad. Sci.* **2011**, *108*, 5021–5026.
(17) Kurokawa, M.; Kim, J.; Geradts, J.; Matsuura, K.; Liu, L.; Ran, X.; Xia, W.; Ribar, T. J.; Henao, R.; Dewhirst, M. W.; et al. A Network of Substrates of the E3 Ubiquitin Ligases MDM2 and HUWE1 Control Apoptosis Independently of p53. *Sci. Signal.* **2013**, *6*, ra32–ra32.
(18) Xia, W.; Petricoin, E. F.; Zhao, S.; Liu, L.; Osada, T.; Cheng, Q.; Wulfkuhle, J. D.; Gwin, W. R.; Yang, X.; Gallagher, R. I.; et al. An Heregulin-EGFR-HER3 Autocrine Signaling Axis Can Mediate Acquired Lapatinib Resistance in HER2+ Breast Cancer Models. *Breast Cancer Res.* **2013**, *15*, R85.
(19) Ladd, D. L.; Snow, R. A. Reagents for the Preparation of Chromophorically Labeled Polyethylene Glycol-Protein Conjugates. *Anal. Biochem.* **1993**, *210*, 258–261.
(20) Christian, N. A.; Milone, M. C.; Ranka, S. S.; Li, G.; Frail, P. R.; Davis, K. P.; Bates, F. S.; Therien, M. J.; Ghoroghchian, P. P.; June, C. H.; et al. Tat-Functionalized Near-Infrared Emissive Polymersomes for Dendritic Cell Labeling. *Bioconjug. Chem.* **2007**, *18*, 31–40.
(21) Christian, N. A.; Benencia, F.; Milone, M. C.; Li, G.; Frail, P. R.; Therien, M. J.; Coukos, G.; Hammer, D. A. In Vivo Dendritic Cell Tracking Using Fluorescence Lifetime Imaging and Near-Infrared-Emissive Polymersomes. *Mol. Imaging Biol.* **2009**, *11*, 167–177.
(22) Lewis Phillips, G. D.; Li, G.; Dugger, D. L.; Crocker, L. M.; Parsons, K. L.; Mai, E.; Blattler, W. A.; Lambert, J. M.; Chari, R. V. J.; Lutz, R. J.; et al. Targeting HER2-Positive Breast Cancer with Trastuzumab-DM1, an Antibody-Cytotoxic Drug Conjugate. *Cancer Res.* **2008**, *68*, 9280–9290.
(23) Hermanson, G. T. *Bioconjugate Techniques*; 2nd ed.; Elsevier Science: Burlington, 2010.
(24) Qi, W.; Ghoroghchian, P. P.; Li, G.; Hammer, D. A.; Therien, M. J. Aqueous Self-Assembly of Poly(ethylene Oxide)-Block-Poly(ε-Caprolactone) (PEO-B-PCL) Copolymers: Disparate Diblock Copolymer Compositions Give Rise to Nano- and Meso-Scale Bilayered Vesicles. *Nanoscale* **2013**, *5*, 10908–10915.

Appendices

(A) Publication reprint: Aqueous Self-Assembly of Poly(ethylene oxide)-block-Poly(e-caprolactone) (PEO-b-PCL) Copolymers: Disparate Diblock Copolymer Compositions Give Rise to Nano- and Meso-Scale Bilayered Vesicles, W. Qi, P. P. Ghoroghchian, G. Li, D. A. Hammer, and M. J. Therien, *Nanoscale*, **2013**, 5, 10908−10915.

(B) Curriculum vitae: Michael J. Therien, Ph.D.

(C) Curriculum vitae: Neil L. Spector, M.D.

Nanoscale

RSC Publishing

PAPER

View Article Online
View Journal | View Issue

Cite this: *Nanoscale*, 2013, **5**, 10908

Aqueous self-assembly of poly(ethylene oxide)-*block*-poly(ε-caprolactone) (PEO-*b*-PCL) copolymers: disparate diblock copolymer compositions give rise to nano- and meso-scale bilayered vesicles†

Wei Qi,[ab] P. Peter Ghoroghchian,[c] Guizhi Li,[b] Daniel A. Hammer[d] and Michael J. Therien*[a]

Nanoparticles formed from diblock copolymers of FDA approved PEO and PCL have generated considerable interest as *in vivo* drug delivery vehicles. Herein, we report the synthesis of the most extensive family PEO-*b*-PCL copolymers that vary over the largest range of number-average molecular weights (M_n: 3.6–57k), PEO weight fractions (f_{PEO}: 0.08–0.33), and PEO chain lengths (0.75–5.8k) reported to date. These polymers were synthesized in order to establish the full range of aqueous phase behaviours of these diblock copolymers and to specifically identify formulations that were able to generate bilayered vesicles (polymersomes). Cryogenic transmission electron microscopy (cryo-TEM) was utilized in order to visualize the morphology of these structures upon aqueous self-assembly of dry polymer films. Nanoscale polymersomes were formed from PEO-*b*-PCL copolymers over a wide range of PEO weight fractions (f_{PEO}: 0.14–0.27) and PEO molecular weights (0.75–3.8k) after extrusion of aqueous suspensions. Comparative morphology diagrams, which describe the nature of self-assembled structures as a function of diblock copolymer molecular weight and PEO weight fraction, show that in contrast to micron-scale polymersomes, which form only from a limited range of PEO-*b*-PCL diblock copolymer compositions, a multiplicity of PEO-*b*-PCL diblock copolymer compositions are able to give rise to nanoscale vesicles. These data underscore that PEO-*b*-PCL compositions that spontaneously form micron-sized polymersomes, as well as those that have previously been reported to form polymersomes *via* a cosolvent fabrication system, provide only limited insights into the distribution of PEO-*b*-PCL diblocks that give rise to nanoscale vesicles. The broad range of polymersome-forming PEO-*b*-PCL compositions described herein suggest the ability to construct extensive families of nanoscale vesicles of varied bilayer thickness, providing the ability to tune the timescales of vesicle degradation and encapsulant release based on the intended *in vivo* application.

Received 24th June 2013
Accepted 27th August 2013

DOI: 10.1039/c3nr03250g

www.rsc.org/nanoscale

Introduction

Polymersomes (50 nm to 50 μm diameter polymer vesicles) formed from amphiphilic block copolymers have attracted much attention due to their superior mechanical stabilities and chemical properties relative to those of conventional lipid-based vesicles (liposomes) and micelles.[1–5] Polymer vesicles can readily encapsulate water-soluble hydrophilic compounds (drugs, vitamins, fluorophores, *etc.*) inside of their aqueous cavities, but also have been shown to be capable of encapsulating large hydrophobic molecules[5–9] within their thick lamellar membranes. Moreover, the sizes, membrane thicknesses, and stabilities of these synthetic vesicle assemblies can be rationally tuned *via* various preparative methods[3,4] that modulate block copolymer chemical structure, number-average molecular weight, and the ratio of hydrophilic to hydrophobic volume fractions, giving rise to polymersomes with varied characteristics that may be optimized for applications in medical imaging, drug delivery, and for topical cosmetic purposes.[3,5,10]

To date, polymersomes have been formed predominantly from amphiphilic diblock copolymers that include poly(ethylene oxide)-*b*-poly(butadiene) (PEO-*b*-PBD),[2,3,5] poly(ethylene oxide)-*b*-poly(ethylethylene) (PEO-*b*-PEE),[2] poly(styrene)-*b*-poly(ethylene

[a]*Department of Chemistry, French Family Science Center, Duke University, 124 Science Drive, Durham, North Carolina 27708, USA. E-mail: michael.therien@duke.edu; Fax: +1 919 684 1522; Tel: +1 919 660 1670*

[b]*Department of Chemistry, University of Pennsylvania, 231 South 34th Street, Philadelphia, Pennsylvania 19104, USA*

[c]*Dana Farber Cancer Institute, 450 Brookline Avenue, Boston, MA, 02115, USA*

[d]*Department of Bioengineering, School of Engineering and Applied Science, University of Pennsylvania, 3320 Smith Walk, Philadelphia, Pennsylvania 19104, USA*

† Electronic supplementary information (ESI) available: Materials and methods, characterization data. See DOI: 10.1039/c3nr03250g

oxide) (PS-*b*-PEO),[11–13] poly(styrene)-*b*-poly(acrylic acid) (PS-*b*-PAA),[3,11,14] poly(ethylene oxide)-*b*-poly(propylenesulfide) (PEO-PPS),[15–17] poly(2-(methacryloyloxy)-ethylphosphoryl-choline)-*b*-poly(2-(diisopropylamino)ethylmethacrylate) (PMPC-PDPA),[18,19] and poly(styrene)-*b*-poly(isocyanoalanine) (2-thiophene-3-yl-ethyl) amide (PS-PIAT).[20–23] None of these well-established polymersome formulations, however, generates fully biodegradable vesicles *via* aqueous self-assembly. A few biodegradable polymersome compositions have been prepared from amphiphilic diblock copolymers of PEO and aliphatic polyesters/polycarbonates using an organic co-solvent/water injection/extraction method.[24–26] In contrast to polymersome preparative procedures based on self-assembly (*i.e.*, film hydration, bulk hydration, or electroformation), the co-solvent method requires the organic co-solvent to be completely removed from the aqueous polymersome suspension post-assembly.

We have previously reported the generation of polymersomes *via* thin-film hydration of the diblock copolymer PEO(2k)-*b*-PCL(12k);[27] the biomedical utility of PEO-*b*-PCL diblock copolymers is noteworthy in that they contain two previously FDA-approved building blocks, poly(ethylene oxide) (PEO) and poly(ε-caprolactone) (PCL). Unlike degradable polymersomes formed from blending "bio-inert" and hydrolysable components,[28,29] PEO-*b*-PCL-based vesicles are fully bioresorbable,[30] leaving no potentially toxic byproducts upon their degradation. In contrast to other degradable (polypeptide-, polyester-, or polyanhydride-based) polymersomes,[24,25,31–33] PEO(2k)-*b*-PCL(12k)-based vesicles are formed through spontaneous self-assembly of the pure amphiphilic diblock copolymer, offering manufacturing advantages in terms of cost and safety. Further, these fully bioresorbable polymersomes possess *in vivo* drug release kinetics appropriate for potential intravascular drug delivery applications.[27]

It is well known that particle sizes greatly influence blood circulation times, reticuloendothelial system (RES) recognition, biodistribution, and the mechanisms of cell uptake.[34–36] The *in vivo* uptake of particles and their extent of drug release increase with decreasing particle sizes and increasing particle surface-area-to-volume ratios.[37–39] As the optimal particle size for prolonged blood stream circulation is ~80–150 nm, and the intracellular uptake of particles having diameters larger than 1 μm is minimal,[37–39] nanometer-sized bioresorbable vesicles are critical for *in vivo* drug delivery of encapsulated therapeutics. Congruent with these requirements, Butler and coworkers[25] have further examined the formation of nano-sized vesicles from a handful of commercially available PEO-*b*-PCL block copolymer compositions featuring mostly small PEO chain lengths (300–2000) and low copolymer molecular weights (M_w: 2.6–7.8k) by the co-solvent injection method.[25]

Expanding upon our initial work,[27] as well as the studies by Butler and colleagues,[25] we describe herein the development of an extensive family of amphiphilic poly(ethylene oxide)-*b*-polycaprolactone (PEO-*b*-PCL) diblock copolymers with varying hydrophilic PEO block weight fractions (f_{PEO}: 0.08–0.33) and PEO chain lengths (0.75–5.8k); we further screened their ability to assemble into bilayered vesicles through aqueous self-assembly of their respective dry polymer films deposited on Teflon™. These biodegradable PEO-*b*-PCL diblock copolymers were fabricated by: (i) ring-opening polymerization of ε-caprolactone monomer (ε-CL) followed by coupling to commercially available monomethoxyl PEO (MePEO), and (ii) sequential anionic living polymerization of PEO and ε-CL monomers. The synthesized PEO-*b*-PCL diblock copolymers possessed number-average molecular weights spanning 3.6–57k, PEO block weight fractions ranging from 0.08–0.33, and polydispersity indices (PDIs) ranging between 1.14 and 1.37 (ESI†). The generated morphologies of PEO-*b*-PCL copolymers prepared *via* self-assembled thin-film rehydration techniques were examined. Comparative morphology diagrams that describe the nature of self-assembled structures as a function of diblock copolymer molecular weight and PEO weight fraction exhibit dramatic differences for the nano- and meso-scale size domains. These studies demonstrate that in contrast to the single diblock copolymer formulation of PEO(2k)-*b*-PCL(12k) (PDI = 1.21) that produces quantitatively micron-sized polymersomes, nanoscale polymersomes can be formed from a multiplicity of PEO-*b*-PCL diblock copolymer compositions under thin-film rehydration conditions.

Experimental

Polymersome preparation

The thin-film hydration method was employed to assemble the PEO-*b*-PCL copolymers into their equilibrium aqueous morphologies. Thin-film hydration has been extensively utilized for preparing non-biodegradable polymersomes comprised of PEO-*b*-PBD diblock copolymers *via* aqueous self-assembly;[5] an analogous protocol was employed herein for experiments involving PEO-*b*-PCL copolymers. An organic solution containing the dissolved biodegradable polymer (200 μL of 7 mg mL^{-1} polymer in $CHCl_3$) was uniformly coated on the surface of a roughened Teflon™ plate followed by vacuum evaporation for >12 h. Addition of an aqueous solution (*e.g.*, DI water) and heating at 60 °C for 48 h led to spontaneous budding of giant (5–20 μm) biodegradable polymersomes into suspension. In polymersome samples that contained 1 mol% Nile Red, the dye was incorporated into the hydrophobic vesicle bilayer during the self-assembly process noted above, which enabled facile visualization of resultant copolymer aqueous morphology *via* confocal fluorescence microscopy (ESI†). Nanoscale unilamellar polymersomes were prepared *via* procedures analogous to those used to formulate small lipid vesicles (sonication, freeze–thaw extraction and extrusion). The sonication procedure involved placing a sample vial containing the aqueous-based solution and a dried thin-film formulation (of polymer uniformly deposited on Teflon™) into a bath sonicator (Fischer Scientific; Model FS20) with constant agitation for 2 h. Freeze–thaw extraction cycles (10) were carried out by alternatively placing the sample vials in liquid N_2 and warm water baths. A narrow size distribution of nano-sized polymersomes was achieved with 3 extrusions using a Liposofast Basic hand-held extruder equipped with 400 nm polycarbonate membranes (Avestin Inc., Ottawa, Ontario). These nano-sized polymersomes were lyophilized and subject to chromatographic purification (PLgel 5 μm

mixed C, 300 × 7.5 mm, linear MW operating range: 200–2 000 000 g mol^{-1}) in order to verify that no measurable PCL hydrolysis of the PEO-*b*-PCL polymers occurred under these experimental conditions.

Results and discussion

Synthesis and characterization of biodegradable PEO-*b*-PCL diblock copolymers

A series of PEO-*b*-PCL diblock copolymers (Table 1) were synthesized (ESI†) *via* ring-opening polymerization of ε-CL and commercially available MePEO (M_n = 5000, 2000, 1100 and 750). MePEO homopolymers bearing one hydroxyl end group were used as the macroinitiator to activate polymerization (130 °C, 24 h) of ε-CL monomer in the presence of catalyst (tin octanoate, $SnOct_2$). PEO-*b*-PCL diblock copolymers have been previously synthesized under a variety of catalyzed[24,40–42] and non-catalyzed conditons.[43,44] Non-catalyzed ring-opening polymerization of ε-CL must, however, be carried out ≥180 °C over several days, which is cumbersome. Of the previously established catalysts, $SnOct_2$ is the most widely used for the production of biodegradable polyesters, as it is commercially available, easy to handle, soluble in common organic solvents and neat liquids (*e.g.*, cyclic ester monomers), and is a permitted food additive in numerous countries.[45–48]

Although the synthesis of PEO-*b*-PCL copolymers from MePEO *via* ring-opening polymerization of ε-CL is facile, the availability of MePEO homopolymers is limited. As such, we utilized anionic living polymerization of ethylene oxide monomers to produce PEOs over an expansive range of molecular weights (M_w); subsequent ε-CL polymerization yields PEO-*b*-PCL copolymers that vary over the largest range of number-average molecular weights (M_n: 3.6–57k) and PEO weight fractions (f_{PEO}: 0.08–0.33) reported to date. An additional advantage of this approach is that the functionality of the PEO terminus of the PEO-*b*-PCL copolymer can be easily varied (ESI, Scheme S2†). These ethylene oxide polymerization reactions utilized cyanomethyl potassium as the protected initiator, which was prepared by metalation of acetonitrile with potassium naphthalenide in THF.[49–52] While anionic living polymerization had been utilized previously in the syntheses of low molecular weight, high PEO weight fraction PEO-*b*-PCL copolymers [*e.g.*, PEO(2.2k)-*b*-PCL(1.2k)],[52] this strategy, as presented herein, also provides PEO-*b*-PCL copolymers that possess a larger range of PEO block molecular weights (1.5, 2.6, 3.0, 3.8, and 5.8 kDa), low PEO weight fractions (f_{PEO}: 0.10–0.23), and a wider range of diblock M_n (7.8–47k) than has been explored previously. ^{1}H NMR spectroscopy was utilized to characterize the number-average molecular weight of the PEO homopolymers and the corresponding PEO-*b*-PCL diblock copolymers (ESI†).[24,40–44,50] GPC was employed to characterize the molecular weight (M_w) and molecular weight distribution (M_w/M_n) (PDI) of each PEO-*b*-PCL diblock copolymer formulation (see ESI†). GPC data indicate that PEO-*b*-PCL diblock copolymers synthesized by anionic living polymerization, having PEO molecular weights of 2.6, 3, 3.8 and 5.8k, exhibited the narrowest molecular weight distributions (PDI: 1.2–1.27). PEO-*b*-PCL diblock copolymers

Table 1 Comparative self-assembled meso-scale morphologies of PEO-*b*-PCL diblock copolymers (PEO: 0.75–5.8k) prepared *via* thin-film hydration and their corresponding nanoscale morphologies observed in aqueous suspension

PEO-*b*-PCL copolymers[a]	f_{PEO}[b]	Morphology[c] (μm)	Morphology[d] (nm)
PEO(0.75k)-*b*-PCL(2.9k)	0.21	MS, IP	V, S
PEO(0.75k)-*b*-PCL(5.8k)	0.11	IP	S
PEO(0.75k)-*b*-PCL(9k)	0.07	IP	P
PEO(1.1k)-*b*-PCL(2.9k)	0.27	MS, IP	V, S
PEO(1.1k)-*b*-PCL(3.7k)	0.23	MS, IP	V, S
PEO(1.1k)-*b*-PCL(6.3k)	0.15	MS, IP	V, S
PEO(1.1k)-*b*-PCL(7.0k)	0.14	IP, MS	V, S
PEO(1.1k)-*b*-PCL(7.7k)	0.12	IP	S, V
PEO(1.1k)-*b*-PCL(9.5k)	0.1	IP	S
PEO(1.1k)-*b*-PCL(13.0k)	0.08	IP	P
PEO(1.5k)-*b*-PCL(6.3k)	0.19	MS, IP	V, S
PEO(1.5k)-*b*-PCL(10.4k)	0.13	IP	S, V
PEO(1.5k)-*b*-PCL(12.4k)	0.11	IP	S
PEO(1.5k)-*b*-PCL(13.7k)	0.1	IP	S
PEO(2k)-*b*-PCL(7.4k)	0.21	IP, MS	V, S
PEO(2k)-*b*-PCL(9.5k)	0.17	V, IP	V, S
PEO(2k)-*b*-PCL(12k)	0.14	V, IP	V, S
PEO(2k)-*b*-PCL(15k)	0.12	IP, V	S, V
PEO(2k)-*b*-PCL(18k)	0.1	IP	S, V
PEO(2k)-*b*-PCL(22k)	0.08	IP	P
PEO(2.6k)-*b*-PCL(11.2k)	0.19	V, IP	V, S
PEO(2.6k)-*b*-PCL(12.3k)	0.17	IP, V	V, S
PEO(2.6k)-*b*-PCL(13.9k)	0.16	IP, V	V, S
PEO(2.6k)-*b*-PCL(15.5k)	0.14	IP, V	S, V
PEO(3k)-*b*-PCL(16.5k)	0.15	IP, V	V, S
PEO(3k)-*b*-PCL(19k)	0.14	IP, V	S, V
PEO(3k)-*b*-PCL(20.5k)	0.13	IP, V	S, V
PEO(3k)-*b*-PCL(24.7k)	0.11	IP	S, P
PEO(3k)-*b*-PCL(25.8k)	0.1	IP	S, P
PEO(3.8k)-*b*-PCL(17k)	0.18	IP, V	V, S
PEO(3.8k)-*b*-PCL(17.7k)	0.17	IP, V	V, S
PEO(3.8k)-*b*-PCL(20k)	0.16	IP, V	S, V
PEO(3.8k)-*b*-PCL(22.2k)	0.15	IP, V	S, V
PEO(5k)-*b*-PCL(10k)	0.33	MS, IP	S
PEO(5k)-*b*-PCL(16k)	0.24	MS, IP	S
PEO(5k)-*b*-PCL(22k)	0.18	IP	S
PEO(5k)-*b*-PCL(26k)	0.16	IP	S
PEO(5k)-*b*-PCL(32k)	0.14	IP	S, P
PEO(5k)-*b*-PCL(52k)	0.09	IP	P
PEO(5.8k)-*b*-PCL(23.8k)	0.2	MS, IP	S
PEO(5.8k)-*b*-PCL(24k)	0.19	MS, IP	S
PEO(5.8k)-*b*-PCL(30.2k)	0.16	IP	S
PEO(5.8k)-*b*-PCL(33.6k)	0.15	IP	S
PEO(5.8k)-*b*-PCL(37.7k)	0.13	IP	S, P
PEO(5.8k)-*b*-PCL(41.2k)	0.12	IP	S, P

[a] Number-average molecular weight of PEO-*b*-PCL diblock copolymers as determined by ^{1}H NMR spectroscopy. [b] Weight fraction of the PEO block as determined by ^{1}H NMR data. [c] Morphology of particles determined qualitatively from fluorescence confocal microscopic studies of the self-assembled structures formed from thin-film rehydration of 50 : 1 molar ratios of copolymer: Nile Red. Observed polymersome and irregularly shaped particle (IP) diameters ranged from less than 1 μm to greater than 30 μm; microsphere (MS) diameters ranged from ~5–30 μm; vesicle (V) diameters spanned ~5–50 μm. In the cases of mixed morphologies, the major component is reported first. [d] Morphologies of particles determined qualitatively from cryogenic transmission electron microscopic studies of the self-assembled structures formed from thin-film rehydration of 50 : 1 molar ratios of copolymer: Nile Red followed by extrusion through a 400 nm porous membrane (S = spherical micelles, V = vesicle, P = precipitate; for systems exhibiting mixed morphologies, the majority component is reported first). See Tables S3 and S4.

synthesized from PEO(2k) *via* ring-opening polymerization showed narrow molecular weight distributions (PDI: 1.1–1.2), while copolymers derived from PEO(5k) displayed distributions that were slightly wider (PDI: 1.32–1.37). These data establish that anionic living polymerization provides an excellent route for the synthesis of PEO-*b*-PCL diblock copolymers with controlled PEO chain length, modulated PEO/PCL block ratio, and narrow molecular weight distribution (see ESI†).

Aqueous morphologies of meso-scale PEO-*b*-PCL diblock copolymers

The thin-film hydration method was preferentially utilized to assemble meso-scale amphiphilic PEO-*b*-PCL diblock copolymers into their equilibrium aqueous morphologies (ESI, Table S1†).[53] Data compiled in Table 1 describe the observed aqueous morphologies for the comprehensive set of PEO-*b*-PCL diblock copolymers that were fabricated; note that extensive microscopy studies (confocal, TEM) demonstrate that preparations of micron-sized polymersomes gave rise to no measurable quantity of corresponding nanoscale structures.

Large numbers of meso-scale polymersomes were obtained from aqueous hydration and self-assembly of the PEO(2k)-*b*-PCL(12k) diblock copolymer ($f_{PEO} = 0.14$) (ESI, Fig. S3†). These polymersomes possessed both multilamellar and unilamellar bilayered structures. In contrast, micron-sized polymersomes were found to coexist with irregular particles in aqueous preparations of PEO(2–3.8k)-*b*-PCL(9.5–22.2k) diblock copolymers, where f_{PEO} ranges between 0.12 and 0.19. In aqueous suspensions of PEO-*b*-PCL diblock copolymers derived from higher (5k or 5.8k) or lower (750–1.5k) molecular weight PEO blocks, no polymersomes were observed regardless of the PEO/PCL ratio (Fig. 1). Unlike conventional vesicle-generating PEO-*b*-PBD copolymers that have a broad range of compositions compatible with high yields of self-assembled meso-scale vesicles, the range of the PEO weight fraction (f_{PEO}: 0.12–0.19), PEO block size (2–3.8k), and total diblock M_n (1.5–26k) compatible with meso-scale polymersome formation for PEO-*b*-PCL diblock copolymers is relatively narrow (Fig. 1). The reduced PEO weight fractions of these polymersome-forming PEO-*b*-PCL compositions ($f_{PEO} = 0.14$) contrast sharply to the PEO-*b*-poly(ethylethylene) and PEO-*b*-poly(butadiene) diblock formulations that give rise to the archetypal polymersomal structure (f_{PEO}: 0.28–0.39).[4,54] The lower PEO weight fractions necessary to generate PCL- and related biodegradable copolymer-based polymersomes may be related to the higher phase transition temperatures for these compositions.[27,55]

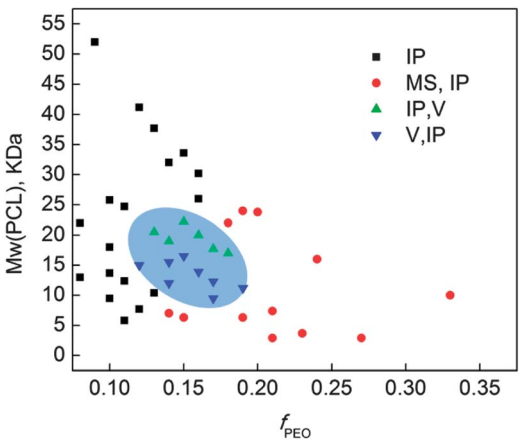

Fig. 1 Phase diagram of micron-sized particles derived from aqueous hydration of PEO-*b*-PCL copolymers. Morphologies were determined qualitatively from fluorescence confocal microscopic studies of the self-assembled structures formed from thin film rehydration of 50 : 1 molar ratios of copolymer : Nile Red. Observed polymersome and irregularly shaped particle (IP) diameters ranged from less than 1 μm to greater than 30 μm; microsphere (MS) diameters ranged from ~5–30 μm; vesicles (V) diameters spanned ~5–50 μm. For systems exhibiting mixed morphologies, the major component is reported first.

Note, in this regard, Discher and coworkers have also studied the meso-scale morphologies generated from a series of PEO-*b*-PCL diblock copolymers using organic co-solvent evaporation;[53] their work focused upon polymeric compositions that featured PEO/PCL ratios that enabled the formation of worm-like micelles; their results, however, differ from those obtained with the experiments carried out with the broader selection of PEO-*b*-PCL diblock compositions examined herein, which describe f_{PEO}, PEO block size, and total diblock M_n ranges that give rise to meso-scale polymersomal morphologies. Note, for example, that the PEO(2k)-*b*-PCL(12k) diblock copolymer composition forms largely worm-like structures *via* the solvent evaporation method,[53] but quantitatively self-assembles into vesicles *via* thin-film hydration (ESI†, Fig. S3). Likewise, (i) PEO(5k)-*b*-PCL(10k) forms vesicles and spheres *via* solvent evaporation,[53] but self-assembles into microspheres *via* the thin-film hydration method (Fig. S4†), and (ii) PEO(5.8k)-*b*-PCL(24k), which has been previously shown to form meso-scale vesicles *via* solvent injection,[24] yields no polymersomes by thin-film hydration. These data indicate that the aqueous morphologies of PEO-*b*-PCL copolymers are sensitive to preparative method and experimental conditions, which may alter the local arrangement of polymer chains that form corresponding aqueous structures. In this regard, the organic co-solvent water injection/extraction method is well known to produce kinetically trapped morphologies that are sensitive to the order of addition, concentrations and ratios of copolymer and solvent, as well as the injection flow rate.[56]

In order to elucidate the effects of diblock copolymer molecular weight distribution on vesicle formation, PEO-*b*-PCL diblock copolymers with varying PEO block size (2.6k, 3k or 3.8k) and narrow molecular distributions (PDI = 1.1) were separated by GPC; no further improvement in the yield of vesicles from these samples was observed relative to PEO-*b*-PCL diblock copolymers of the same molecular weight having slightly broader molecular weight distributions (PDI: 1.2–1.4). Similarly, the polymersome-forming abilities of PEO-*b*-PCL diblock copolymer mixtures having much wider molecular weight distributions were examined; scanning laser confocal microscopy of such samples (Fig. 2), shows that polymersomes can be obtained in high yield from a 1 : 1 : 1 PEO(2k)-*b*-PCL(9.5k) : PEO(2k)-*b*-PCL(12k) : PEO(2k)-*b*-PCL(15k) copolymer blend, suggesting that the molecular weight distribution has little influence on biodegradable polymersome formation from mixtures containing a significant weight fraction of the PEO(2k)-*b*-PCL(12k) diblock copolymer.

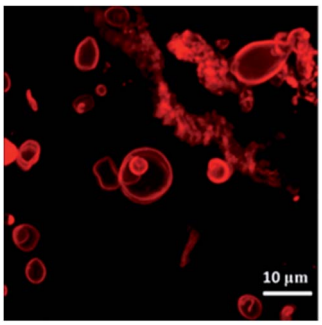

Fig. 2 Scanning fluorescence confocal micrograph ($\lambda_{ex} = 488$ nm) of polymersomes derived from a 1 : 1 : 1 mixture of PEO(2k)-*b*-PCL(9.5k), PEO(2k)-*b*-PCL(12k), and PEO(2k)-*b*-PCL(15k), containing membrane-encapsulated Nile Red (peak emission = 603 nm) in DI water at 25 °C.

Nanoscale morphologies of self-assembled PEO-*b*-PCL diblock copolymers in aqueous suspension

Nanoscale polymersomes are formed from dry thin-films of PEO-*b*-PCL deposited on Teflon™ upon rehydration in an aqueous solution, along with the addition of sonic energy; several subsequent cycles of freeze–thaw extraction and extrusion (Fig. 3 and 4; see Experimental section, ESI†) yield vesicles of a desired size with narrow distribution (*e.g.* $d \sim 100 \pm 15$ nm). Solution morphologies were characterized utilizing cryo-TEM, which allowed for direct visualization of the aggregate nano-sized structures formed in aqueous suspension (Table 1); note that dynamic light scattering (DLS) measurements confirmed the homogeneous size distributions and were consistent with cryo-TEM experimental data. Nanoscale polymersomes are formed from PEO-*b*-PCL diblock copolymers of a range of PEO weight fractions (f_{PEO}: 0.14–0.27) and block sizes (PEO 0.75–3.8k). Butler *et al.*[25] examined a few low molecular weight PEO-*b*-PCL copolymers that assembled into nm-sized morphologies *via* co-solvent injection; the results of these investigators mirror the Table 1 data for low molecular weight PEO-*b*-PCL polymers (f_{PEO}: 0.14–0.27 and PEO molecular weights of 0.75–3.8k) that form nanoscale vesicles *via* self-assembly after thin-film hydration. Note, however, for high molecular weight PEO-*b*-PCL copolymers with PEO block molecular weight over 3.8k, such as PEO(5k, 5.8k)-PCL diblock copolymers, only spherical micelles and particles are formed under thin-film hydration conditions over a large range of PEO weight fractions (f_{PEO}: 0.09–0.33). It is important to underscore that significant morphological differences are evident for self-assembled meso- and nanoscale structures for a given PEO-*b*-PCL diblock copolymer. In contrast to morphologies generated on the meso scale, polymersomes dominate observed self-assembled nanoscale morphologies of these PEO-*b*-PCL diblock copolymers, suggesting disparate formation mechanisms for nano- and meso-sized polymersomes that form under thin film hydration conditions.

As shown in Fig. 5, both hydrophilic volume fraction and PEO chain length affect the observed distribution of self-assembled morphologies on the nanoscale. To further explore this issue, several PEO-*b*-PCL diblock copolymers were

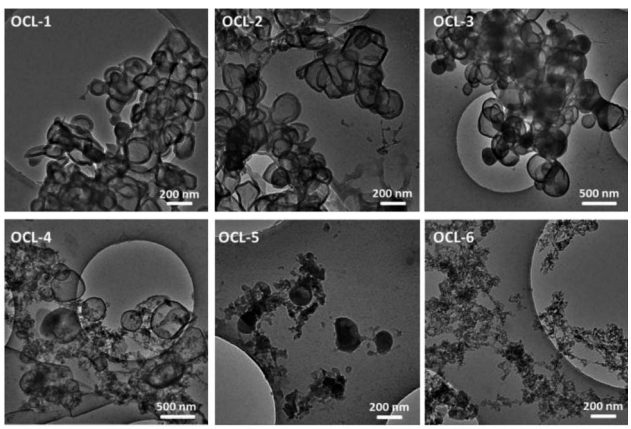

	OCL Copolymers	f_{PEO}	Extent to which vesicles comprise the visually observed morphologies
OCL-1	PEO(2K)-b-PCL(7.4K)	0.21	D
OCL-2	PEO(2K)-b-PCL(9.5K)	0.17	D
OCL-3	PEO(2K)-b-PCL(12K)	0.14	D
OCL-4	PEO(2K)-b-PCL(15K)	0.12	C
OCL-5	PEO(2K)-b-PCL(18K)	0.10	A
OCL-6	PEO(2K)-b-PCL(22K)	0.08	None

Fig. 3 Cryo-TEM images of nanoscale polymersomes derived from PEO-*b*-PCL (OCL) diblock copolymers. Aqueous suspensions of OCL 1–6 were generated *via* thin-film hydration and subsequent self-assembly. D (dominant morphology): vesicles define the most prevalently observed morphological structure; C (common morphology): vesicles define one of the commonly observed morphological structures; A (atypical morphology): vesicles are observed, but such structures are less common than other observed morphologies.

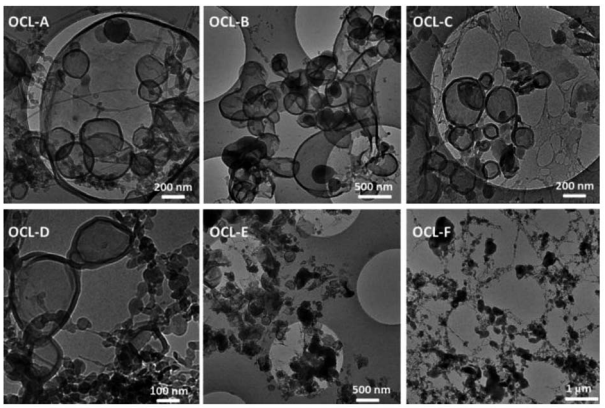

	OCL Copolymers	f_{PEO}	Extent to which vesicles comprise the visually observed morphologies
OCL-A	PEO(1.1K)-*b*-PCL(6.3K)	0.15	D
OCL-B	PEO(2K)-*b*-PCL(12K)	0.14	D
OCL-C	PEO(2.6K)-*b*-PCL(15.5K)	0.14	D
OCL-D	PEO(3K)-*b*-PCL(16.5K)	0.15	C
OCL-E	PEO(3.8K)-*b*-PCL(22.2K)	0.15	A
OCL-F	PEO(5K)-*b*-PCL(27K)	0.15	A

Fig. 4 Cryo-TEM images of nanoscale polymersomes derived from PEO-*b*-PCL (OCL) diblock copolymers. Aqueous suspensions of OCL A–F were generated *via* thin-film hydration and subsequent self-assembly. D (dominant morphology): vesicles define the most prevalently observed morphological structure; C (common morphology): vesicles define one of the commonly observed morphological structures; A (atypical morphology): vesicles are observed, but such structures are less common than other observed morphologies.

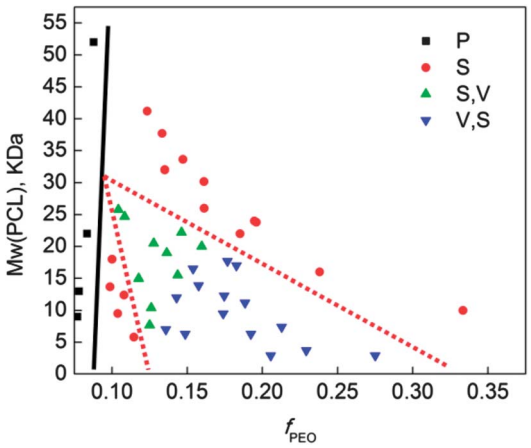

Fig. 5 Phase diagram of nanoscale particles derived from aqueous hydration of PEO-*b*-PCL copolymers. Morphologies were determined qualitatively from cryogenic transmission electron microscopic studies of the self-assembled structures formed from thin film rehydration of 50 : 1 molar ratios of copolymer : Nile Red followed by extrusion through a 400 nm porosity membrane (S = spherical micelles, V = vesicle, P = precipitate; for systems exhibiting mixed morphologies, the major component is noted first).

generated that featured the same PEO chain length (2k) but which differed with respect to hydrophilic PEO weight fraction (see OCL 1–6 in Fig. 3); further, other PEO-*b*-PCL copolymers were also synthesized that exhibited identical PEO weight fractions, but which differed with respect to PEO chain length (see OCL A–E in Fig. 4). The data chronicled in Fig. 3 demonstrate that increasing the molecular weight of the PCL block at a constant PEO chain length (f_{PEO}: 0.21 → 0.08) results in a morphological transition from bilayered vesicles to micellar aggregates. Increasing the length of PCL block augments the hydrophobic content of the amphiphile while decreasing the interfacial curvature, leading to the development of micellar morphologies. Fig. 4 highlights that uniform spherical vesicles are formed from PEO(2k)-*b*-PCL diblock copolymers when $0.21 < f_{PEO} < 0.12$, with micelles first appearing when f_{PEO} falls below 0.14. For PEO-*b*-PCL diblock copolymers with f_{PEO} fixed at ~15%, PEO chain lengths ranging from 1.1 to 3.8k support polymersome formation at the nanoscale, while micellar aggregates are evident for diblocks having PEO molecular weights <1.1k or >3k.

It is well known that the morphology of diblock copolymer assemblies is determined by the interfacial curvature of the amphiphile;[52] moreover, previous work has revealed that the surface elasticity of bilayer membranes is scale independent and only depends on the interface.[4,57] It is the expectation, therefore, that self-assembled diblock copolymer morphologies elucidated at one size domain provide predictive insights into morphologies that will be evident over other size domains. While this has shown to be true for meso-scale and larger bilayered vesicles, these data emphasize that it is incorrect to extend such predictions to the nanoscale. While the origin of this effect can only be discussed qualitatively, it is likely that the dramatically increased total surface areas and correspondingly decreased surface tensions characteristic of nanoscale bilayered vesicles serve to mitigate destabilizing effects that derive from the augmented interfacial curvature required for vesicle formation, relative to hypothetical micron-sized vesicles derived from an identical diblock copolymer. Likewise, this observed difference in ability to form mesoscopic *versus* nanoscopic vesicles may stem in part from the crystallinity of the hydrophobic PCL chains.[30] The restricted mobility of the PCL chains may allow the assembly of small sections of bilayers, whereas large length-scale assemblies of lamellar phases may be disallowed. Increased solution energy (*via* heating and sonication) may also allow for the generation of nano-sized vesicles that would otherwise be energetically unfavourable at the mesoscale for a given diblock copolymer composition; upon solution cooling, increased interchain packing may augment stabilization of the bilayered membrane, yielding the final nanoscale structure. The differences between self-assembled morphologies formed at different length scales should thus be systematically explored for different diblock formulations of a given composition in order to determine if this is a universal effect or one that is dependent on polymer chain flexibility and diblock copolymer transition temperatures. In any event, this work demonstrates clearly that if nanoscale vesicles are the targeted design, there is no substitute for direct screening and characterization of diblock polymer compositions that give rise to self-assembled nanoscale morphologies *via* cryo-TEM.

Conclusions

A series of PEO-*b*-PCL diblock copolymers varying in PEO block size (M_n: 750, 1100, 2000 and 5000), f_{PEO} (0.08–0.33), and M_n (3.6–57k) were synthesized by ring-opening polymerization of ε-CL monomer using commercially available MePEO as the macro-initiator; anionic living polymerization was also employed to synthesize PEO-*b*-PCL copolymers with a wider range of controlled PEO block sizes (M_n: 1500, 2600, 3000, 3800, and 5800), f_{PEO} (0.10–0.23), and M_w (ranging from 7.8 to 47k). All copolymers were analysed by GPC and possessed narrow molecular weight distributions (PDI: 1.14–1.37).

The nature of the self-assembled aqueous morphologies derived from these polymers was probed on the micron scale using epifluorescent optical and scanning confocal fluorescence microscopies, and on the nanoscale *via* cryogenic transmission electron microscopy (cryo-TEM). Key morphological differences were observed to exist between self-assembled meso- and nanoscale structures for a given PEO-*b*-PCL diblock copolymer. While a single composition [PEO(2k)-*b*-PCL(12k); PDI = 1.21] provided self-assembled micron-sized structures in which vesicles were the most prevalently observed morphology under thin-film rehydration conditions, corresponding nanoscale polymersomes were formed from a multiplicity of PEO-*b*-PCL diblock copolymer compositions: these included PEO-*b*-PCL copolymers having a wide range of PEO weight fractions (f_{PEO}: 0.1–0.27), as well as PCL molecular weights (3.65–26k).

This work shows, for the first time, that morphological differences exist between self-assembled meso- and nanoscale structures for a given PEO-*b*-PCL diblock copolymer and underscores that PEO-*b*-PCL diblock copolymer compositions

that form meso-scale polymersomes provide only limited insight into the distribution of PEO-*b*-PCL diblocks that give rise to corresponding vesicles on the nanoscale. Because PEO and PCL are FDA-approved polymers, this broad range of polymersome-forming PEO-*b*-PCL compositions suggests a more extensive utility of these species as nanometric drug delivery vehicles, as polymersomal bilayer thicknesses will undoubtedly modulate timescales of vesicle degradation and corresponding release of polymersomal contents in biologically relevant applications.

Acknowledgements

This work was supported by grants from the Department of Defense (W81XWH-13-1-0086), the National Cancer Institute (R01CA115229), and the National Institutes of Health (EB003457-01). M.J.T. and D.A.H. thank the MRSEC Program of the National Science Foundation (DMR-00-79909) for infrastructural support.

Notes and references

1 B. M. Discher, Y. Y. Won, D. S. Ege, J. Lee, F. S. Bates, D. E. Discher and D. A. Hammer, *Science*, 1999, **284**, 1143–1146.
2 J. C. M. Lee, H. Bermudez, B. M. Discher, M. A. Sheehan, Y.-Y. Won, F. S. Bates and D. E. Discher, *Biotechnol. Bioeng.*, 2001, **73**, 135–145.
3 D. E. Discher and A. Eisenberg, *Science*, 2002, **297**, 967–973.
4 H. Bermudez, A. K. Brannan, D. A. Hammer, F. S. Bates and D. E. Discher, *Macromolecules*, 2002, **35**, 8203–8208.
5 P. P. Ghoroghchian, P. R. Frail, K. Susumu, D. Blessington, A. K. Brannan, F. S. Bates, B. Chance, D. A. Hammer and M. J. Therien, *Proc. Natl. Acad. Sci. U. S. A.*, 2005, **102**, 2922–2927.
6 P. P. Ghoroghchian, P. R. Frail, K. Susumu, T. H. Park, S. P. Wu, H. T. Uyeda, D. A. Hammer and M. J. Therien, *J. Am. Chem. Soc.*, 2005, **127**, 15388–15390.
7 P. P. Ghoroghchian, J. J. Lin, A. K. Brannan, P. R. Frail, F. S. Bates, M. J. Therien and D. A. Hammer, *Soft Matter*, 2006, **2**, 973–980.
8 P. P. Ghoroghchian, P. R. Frail, G. Li, J. A. Zupancich, F. S. Bates, D. A. Hammer and M. J. Therien, *Chem. Mater.*, 2007, **19**, 1309–1318.
9 T. V. Duncan, P. P. Ghoroghchian, I. V. Rubtsov, D. A. Hammer and M. J. Therien, *J. Am. Chem. Soc.*, 2008, **130**, 9773–9784.
10 F. Meng, G. H. M. Engbers and J. Feijen, *J. Controlled Release*, 2005, **101**, 187–198.
11 K. Yu, L. Zhang and A. Eisenberg, *Langmuir*, 1996, **12**, 5980–5984.
12 K. Yu and A. Eisenberg, *Macromolecules*, 1996, **29**, 6359–6361.
13 K. Yu and A. Eisenberg, *Macromolecules*, 1998, **31**, 3509–3518.
14 H. Shen and A. Eisenberg, *Macromolecules*, 2000, **33**, 2561–2572.
15 F. Ahmed, P. J. Photos and D. E. Discher, *Drug Dev. Res.*, 2006, **67**, 4–14.
16 D. A. Christian, S. Cai, D. M. Bowen, Y. Kim, J. D. Pajerowski and D. E. Discher, *Eur. J. Pharm. Biopharm.*, 2009, **71**, 463–474.
17 O. Onaca, R. Enea, D. W. Hughes and W. Meier, *Macromol. Biosci.*, 2009, **9**, 129–139.
18 H. Lomas, J. Du, I. Canton, J. Madsen, N. Warren, S. P. Armes, A. L. Lewis and G. Battaglia, *Macromol. Biosci.*, 2010, **10**, 513–530.
19 C. Murdoch, K. J. Reeves, V. Hearnden, H. Colley, M. Massignani, I. Canton, J. Madsen, A. Blanazs, S. P. Armes and A. L. Lewis, *Nanomedicine*, 2010, **5**, 1025–1036.
20 S. F. M. van Dongen, M. Nallani, S. Schoffelen, J. J. L. M. Cornelissen, R. J. M. Nolte and J. van Hest, *Macromol. Rapid Commun.*, 2008, **29**, 321–325.
21 S. M. Kuiper, M. Nallani, D. M. Vriezema, J. J. L. M. Cornelissen, J. C. M. van Hest, R. J. M. Nolte and A. E. Rowan, *Org. Biomol. Chem.*, 2008, **6**, 4315–4318.
22 M. Nallani, R. Woestenenk, H.-P. M. de Hoog, S. F. M. van Dongen, J. Boezeman, J. J. L. M. Cornelissen, R. J. M. Nolte and J. C. M. van Hest, *Small*, 2009, **5**, 1138–1143.
23 Z. Fu, M. A. Ochsner, H. P. M. de Hoog, N. Tomczak and M. Nallani, *Chem. Commun.*, 2011, **47**, 2862–2864.
24 F. Meng, C. Hiemstra, G. H. M. Engbers and J. Feijen, *Macromolecules*, 2003, **36**, 3004–3006.
25 D. J. Adams, C. Kitchen, S. Adams, S. Furzeland, D. Atkins, P. Schuetz, C. M. Fernyhough, N. Tzokova, A. J. Ryan and M. F. Butler, *Soft Matter*, 2009, **5**, 3086–3096.
26 A. Johnston, P. Dalton and T. Newman, *J. Nanopart. Res.*, 2010, **12**, 1997–2001.
27 P. P. Ghoroghchian, G. Li, D. H. Levine, K. P. Davis, F. S. Bates, D. A. Hammer and M. J. Therien, *Macromolecules*, 2006, **39**, 1673–1675.
28 F. Ahmed, A. Hategan, D. E. Discher and B. M. Discher, *Langmuir*, 2003, **19**, 6505–6511.
29 F. Ahmed and D. E. Discher, *J. Controlled Release*, 2004, **96**, 37–53.
30 J.-Z. Bei, J.-M. Li, Z.-F. Wang, J.-C. Le and S.-G. Wang, *Polym. Adv. Technol.*, 1997, **8**, 693–696.
31 F. Najafi and M. N. Sarbolouki, *Biomaterials*, 2003, **24**, 1175–1182.
32 E. G. Bellomo, M. D. Wyrsta, L. Pakstis, D. J. Pochan and T. J. Deming, *Nat. Mater.*, 2004, **3**, 244–248.
33 P. Schuetz, M. J. Greenall, J. Bent, S. Furzeland, D. Atkins, M. F. Butler, T. C. B. McLeish and D. M. A. Buzza, *Soft Matter*, 2011, **7**, 749–759.
34 H. Harashima and H. Kiwada, *Adv. Drug Delivery Rev.*, 1996, **19**, 425–444.
35 I. Ueda, J.-S. Chiou, P. R. Krishna and H. Kamaya, *Biochim. Biophys. Acta, Biomembr.*, 1994, **1190**, 421–429.
36 D. C. Drummond, O. Meyer, K. Hong, D. B. Kirpotin and D. Papahadjopoulos, *Pharmacol. Rev.*, 1999, **51**, 691–743.
37 A. T. Florence and N. Hussain, *Adv. Drug Delivery Rev.*, 2001, **50**, S69–S89.
38 W. Sass, H. P. Dreyer and J. Seifert, *Am. J. Gastroenterol.*, 1990, **85**, 255–260.

39 P. G. Jenkins, K. A. Howard, N. W. Blackball, N. W. Thomas, S. S. Davis and D. T. O'Hagan, *J. Controlled Release*, 1994, **29**, 339–350.
40 B. Bogdanov, A. Vidts, A. Van Den Buicke, R. Verbeeck and E. Schacht, *Polymer*, 1998, **39**, 1631–1636.
41 J. J. Zastre, J. Jackson, M. Bajwa, R. Liggins, F. Iqbal and H. Burt, *Eur. J. Pharm. Biopharm.*, 2002, **54**, 299–309.
42 S.-H. Hsu, C.-M. Tang and C. C. C.-C. Lin, *Biomaterials*, 2004, **25**, 5593–5601.
43 P. Cerrai, M. Tricoli, F. Andruzzi, M. Paci and M. Paci, *Polymer*, 1989, **30**, 338–343.
44 Y.-I. Jeong, M.-K. Kang, H.-S. Sun, S.-S. Kang, H.-W. Kim, K.-S. Moon, K.-J. Lee, S.-H. Kim and S. Jung, *Int. J. Pharm.*, 2004, **273**, 95–107.
45 H. R. Kricheldorf, C. Boettcher and K.-U. Tönnes, *Polymer*, 1992, **33**, 2817–2824.
46 G. Schwach, J. Coudane, R. Engel and M. Vert, *J. Polym. Sci., Part A: Polym. Chem.*, 1997, **35**, 3431–3440.
47 A. Kowalski, A. Duda and S. Penczek, *Macromolecules*, 2000, **33**, 7359–7370.
48 C.-M. Dong, K.-Y. Qiu, Z.-W. Gu and X.-D. Feng, *Macromolecules*, 2001, **34**, 4691–4696.
49 S. Cammas, Y. Nagasaki and K. Kataoka, *Bioconjugate Chem.*, 1995, **6**, 226–230.
50 Y. Nagasaki, M. Iijima, M. Kato and K. Kataoka, *Bioconjugate Chem.*, 1995, **6**, 702–704.
51 M. A. Hillmyer and F. S. Bates, *Macromolecules*, 1996, **29**, 6994–7002.
52 M. Deng, R. Wang, G. Rong, J. Sun, X. Zhang, X. Chen and X. Jing, *Biomaterials*, 2004, **25**, 3553–3558.
53 K. Rajagopal, A. Mahmud, D. A. Christian, J. D. Pajerowski, A. E. X. Brown, S. M. Loverde and D. E. Discher, *Macromolecules*, 2010, **43**, 9736–9746.
54 P. J. Photos, L. Bacakova, B. Discher, F. S. Bates and D. E. Discher, *J. Controlled Release*, 2003, **90**, 323–334.
55 J. A. Zupancich, F. S. Bates and M. A. Hillmyer, *Macromolecules*, 2006, **39**, 4286–4288.
56 C. Sanson, C. Schatz, J.-F. Le Meins, A. Brulet, A. Soum and S. Lecommandoux, *Langmuir*, 2010, **26**, 2751–2760.
57 S. Jain and F. S. Bates, *Science*, 2003, **300**, 460–464.

BIOGRAPHICAL SKETCH

NAME	POSITION TITLE
Michael J. Therien	William R. Kenan, Jr. Professor

EDUCATION/TRAINING

INSTITUTION AND LOCATION	DEGREE	YEAR(s)	FIELD OF STUDY
University of California, Los Angeles, CA	B. S.	1982	Chemistry
University of California, San Diego, CA	Ph.D.	1987	Chemistry
California Institute of Technology, Pasadena, CA	NIH PostDoc	1987-1990	Chemistry

RESEARCH AND PROFESSIONAL EXPERIENCE:

Positions Held:

University of Pennsylvania	Assistant Professor	1990-1996
University of Pennsylvania	Associate Professor	1996-1997
University of Pennsylvania	Professor of Chemistry	1997-2002
Princeton University	Visiting Professor	2002
University of Pennsylvania	Alan G. MacDiarmid Professor of Chemistry	2002-2007
Universiteit of Lueven	Visiting Professor	2004; 2005
Universiteit of Leuven	Francqui International Professor	2008-2009
Duke University	Professor of Chemistry	2008
Duke University	William R. Kenan, Jr. Professor	2009-present
University of Bordeaux	Visiting Professor	2010

Honors:

National Institutes of Health Postdoctoral Research Fellow (1987-1990); Searle Scholar (1991-1994); Arnold and Mabel Beckman Foundation Young Investigator (1992-1994); National Science Foundation Young Investigator (1993-1998); E. I. DuPont de Nemours Young Faculty Award (1995-1997); Alfred P. Sloan Foundation Fellow (1995-1997); Camille Dreyfus Teacher-Scholar (1997-2002); Journal of Porphyrins and Phthalocyanines Young Investigator Award (2002); Pederson Lecturer, Central Research and Development Division, E. I. DuPont de Nemours (2003); American Chemical Society Philadelphia Section Award (2004); W. Heinlen Hall Lectureship, Bowling Green State University (2005); Elected Fellow, American Association for the Advancement of Science (2005); International Fancqui Chair, Belgium (2008-2009); Fellow, Flemish Academy of Science (2009).

Advisory Positions:

External Reviewer, United States Department of Energy, Nanotechnology Centers (2003-present); Review Committee Member, Beckman Young Investigator Program (2003-present); Research Team Leader, NSF-supported Nanoscience and Technology Center (2004-2008); Scientific Advisory Board, Center for Nanoscale Materials, Argonne National Laboratory (2005-present); ARPA-E Photovoltaics Review Committee Chair (2009); External Program Reviewer, Scientific Foundation Ireland (2011); Molecular Assemblies Research Team Leader, DOE Energy Frontier Research Center for Solar Fuels (2012-present).

Earlier Publications Pertinent to this Application:

1) Highly-Conjugated, Acetylenyl-Bridged Porphyrins: New Models for Light-Harvesting Antenna Systems, V. S.-Y. Lin, S. G. DiMagno, and M. J. Therien, *Science (Washington, D. C.)* **1994**, *264*, 1105-1111.

2) The Role of Porphyrin-to-Porphyrin Linkage Topology in the Extensive Modulation of the Absorptive and Emissive Properties of a Series of Ethynyl- and Butadiynyl-Bridged Bis- and Tris(porphinato)zinc Chromophores, V. S.-Y. Lin and M. J. Therien, *Chem. Eur. J.* **1995**, *1*, 645-651.
3) Ultrafast Dynamics of Highly Conjugated Porphyrin Arrays, R. Kumble, S. Palese, V. S.-Y. Lin, M. J. Therien, and R. M. Hochstrasser, *J. Am. Chem. Soc.* **1998**, *120*, 11489-11498.
4) NIR-Emissive Polymersomes: Self-assembled Soft Matter for *in vivo* Optical Imaging, P. P. Ghoroghchian, P. R. Frail, K. Susumu, D. Blessington, A. K. Brannan, F. S. Bates, B. Chance, D. A. Hammer, and M. J. Therien, *Proc. Natl. Acad. Sci. U.S.A.* **2005**, *102*, 2922-2927.
5) Near-Infrared Optical Imaging of B16 Melanoma Cells via Low-Density Lipoprotein-Mediated Uptake and Delivery of High Emission Dipole Strength Tris[(Porphinato)Zinc(II)] Fluorophores, S. P. Wu, I. Lee, P. P. Ghoroghchian, P. R. Frail, G. Zheng, J. D. Glickson, and M. J. Therien, *Bioconjugate Chem.* **2005**, *16*, 542-550.
6) Broad Spectral Domain Fluorescence Wavelength Modulation of Visible and Near Infrared-Emissive Polymersomes, P. P. Ghoroghchian, P. R. Frail, K. Susumu, T.-H. Park, S. P. Wu, H. T. Uyeda, D. A. Hammer, and M. J. Therien, *J. Am. Chem. Soc.* **2005**, *127*, 15388-15390.
7) Bioresorbable Vesicles Formed through Spontaneous Self-Assembly of Amphiphilic Polyethyleneoxide-*Block*-Polycaprolactone, P. P. Ghoroghchian, G. Li, D. H. Levine, K. P. Davis, F. S. Bates, D. A. Hammer, and M. J. Therien, *Macromolecules* **2006**, *39*, 1673-1675.
8) Exceptional Near Infrared Fluorescence Quantum Yields and Excited-State Absorptivity of Conjugated Porphyrin Arrays, T. V. Duncan, K. Susumu, L. E. Sinks, and M. J. Therien, *J. Am. Chem. Soc.* **2006**, *128*, 9000-9001.
9) Quantitative Loading, Steady-State Emission, and Mechanical Stability of Near Infrared Emissive Polymersomes, P. P. Ghoroghchian, J. J. Lin, A. K. Brannan, P. R. Frail, F. S. Bates, M. J. Therien, and D. A. Hammer, *Soft Matter* **2006**, *2*, 973-980.
10) Tat-Functionalized Near-Infrared Polymersomes for Dendritic Cell Labeling, N. A. Christian, M. C. Milone, S. S. Ranka, G. Li, P. R. Frail, K. P. Davis, F. S. Bates, M. J. Therien, P. P. Ghoroghchian, C. H. June, and D. A. Hammer, *Bioconjugate Chem.* **2007**, *18*, 31-40.
11) Controlling Bulk Optical Properties of Emissive Polymersomes Through Intramembranous Polymer-Fluorophore Interactions, P. P. Ghoroghchian, P. R. Frail, G. Li, J. A. Zupancich, F. S. Bates, D. A. Hammer, and M. J. Therien, *Chem. Mater.* **2007**, *19*, 1309-1318.
12) Ultrafast Excited State Dynamics of Nanoscale Near Infrared Emissive Polymersomes, T. V. Duncan, P. P. Ghoroghchian, I. V. Rubstov, D. A. Hammer, and M. J. Therien, *J. Am. Chem. Soc.* **2008**, *130*, 9773-9784.
13) Using -Helical Coiled-Coils to Design Nanostructured Porphyrin Arrays, K. A. McAllister, H. Zou, F. V. Cochran, G. M. Bender, A. Senes, H. C. Fry, V. Nanda, P. A. Keenan, J. D. Lear, M. J. Therien, J. K. Blasie, and W. F. DeGrado, *J. Am. Chem. Soc.* **2008**, *130*, 11921–11927.
14) Leuko-Polymersomes, D. A. Hammer, G. R. Robbins, J. J. Lin, L. A. Smith, P. P. Ghoroghchian, M. J. Therien, and F. S. Bates, *Faraday Discuss.* **2008**, *139*, 129–141.
15) Polymersomes: A New Multi-Functional Tool for Cancer Diagnosis and Therapy, D. H. Levine, P. P. Ghoroghchian, J. Freudenberg, G. Zhang, M. J. Therien, M. I. Greene, D. A. Hammer, and R. Murali, *Methods* **2008**, *46*, 25-32.
16) In Vivo Fluorescence Imaging: A Personal Perspective, P. P. Ghoroghchian, M. J. Therien, and D. A. Hammer, *Wiley Interdisciplinary Reviews: Nanomedicine and Nanobiotechnology*, **2009**, *1*, 156-167.
17) Photo-initiated Destruction of Composite Porphyrin-Protein Polymersomes, M. Jimbo, G. P. Robbins, J. Swift, M. J. Therien, D. A. Hammer, and I. J. Dmochowski, *J. Am. Chem. Soc.* **2009**, *131*, 3872–3874.
18) In Vivo Dendritic Cell Tracking Using Fluorescence Lifetime Imaging and Near-Infrared Emissive Polymersomes, N. A. Christian, F. Benencia, M. C. Milone, G. Li, P. R. Frail, M. J. Therien, G. Coukos, and D. A. Hammer, *Molecular Imaging & Biology* **2009**, *11*, 167-177.
19) How to Improve Your Image, M. J. Therien, *Nature (London)* **2009**, *458*, 716-717.

20) Tunable Leuko-polymersomes that Adhere Specifically to Inflammatory Markers, G. P. Robbins, R. L. Saunders, J. B. Haun, J. Rawson, M. J. Therien, and D. A. Hammer, *Langmuir* **2010**, *26*, 14089–14096.
21) A Generalized System for Photo-Responsive Membrane Rupture in Polymersomes, N. P. Kamat, G. P. Robbins, J. Rawson, M. J. Therien, I. J. Dmochowski, and D. A. Hammer, *Adv. Funct. Mater.* **2010**, *20*, 2588–2596.
22) Effects of Membrane Rheology on Leuko-polymersome Adhesion to Inflammatory Ligands, G. P. Robbins, D. Lee, J. S. Katz, P. R. Frail, M. J. Therien, J. C. Crocker, D. A. Hammer, *Soft Matter* **2011**, *7*, 769–779.
23) Sensing Membrane Stress with Near IR-emissive Porphyrins, N. P. Kamat, Z. Liao, L. E. Moses, J. Rawson, M. J. Therien, I. J. Dmochowski, and D. A. Hammer, *Proc. Natl. Acad. Sci. U.S.A.* **2011**, *108*, 13984–13989.
24) Upconversion Luminescence and X-Ray Excited Scintillation from Single-Composition Rare-Earth Doped Yttrium Oxide Nanocrystals, I. N. Stanton, J. A. Ayres, and M. J. Therien, *Dalton Trans.* **2012**, *41*, 11576–11578.
25) Soft Biodegradable Polymersomes from Caprolactone-Derived Polymers, J. S. Katz, K. A. Eisenbrown, E. D. Johnston, N. P. Kamat, J. Rawson, M. J. Therien, J. A. Burdick, and D. A. Hammer, *Soft Matter*, **2012**, *37*, 10853–10862.
26) Biodegradable Polymersomes for the Delivery of Gemcitabine to Panc-1 Cells, N. Sood, W. T. Jenkins, X.-Y. Yang, N. N. Shah, J. S. Katz, C. J. Koch, P. R. Frail, M. J. Therien, D. A. Hammer, and S. M. Evans, *J. Pharmaceutics,* **2013**, 932797.
27) Aqueous Self-Assembly of Poly(ethylene oxide)-block-Poly(-caprolactone) (PEO-b-PCL) Copolymers: Disparate Diblock Copolymer Compositions Give Rise to Nano- and Meso-Scale Bilayered Vesicles, W. Qi, P. P. Ghoroghchian, G. Li, D. A. Hammer, and M. J. Therien, *Nanoscale*, **2013**, 5, 10908**–**10915.
28) Antibody-Targeted Near-Infrared Emissive Polymersomes: Sensitive Nanoscale Agents for in vitro Diagnostics and Imaging, W. Qi, D. R. Fels, J. T. Stecher, M. W. Dewhirst, and M. J. Therien, *Nature Materials*. Submitted.

Exemplary Additional Publications over the Three Previous Years (2011-2013):

29) The Roles of Molecular Structure and Effective Optical Symmetry in Evolving Dipolar Chromophoric Building Blocks to Potent Octopolar NLO Chromophores, T. Ishizuka, L. E. Sinks, K. Song, S.-T. Hung, A. Nayak, K. Clays, and M. J. Therien, *J. Am. Chem. Soc.* **2011**, *133*, 2884–2896.
30) Electron Transfer Reactions of Rigid, Cofacially Compressed, π-Stacked Porphyrin-Bridge-Quinone Systems, Y. K. Kang, P. M. Iovine, and M. J. Therien, *Coord. Chem. Rev.* **2011**, *255*, 804-824.
31) Two-Photon Absorption Properties of Proquinoidal D-A-D and A-D-A Quadrupolar Chromophores, K. Susumu, J. A. N. Fisher, J. Zheng, D. N. Beratan, A. G. Yodh, and M. J. Therien, *J. Phys. Chem. A.* **2011**, *115*, 5525–5539.
32) Controlling Polarization Dependent Reactions to Fabricate Multi-Component Functional Nanostructures, D. Conklin, T.-H. Park, S. Nanayakkara, M. J. Therien, and D.A. Bonnell, *Adv. Funct. Mater.* **2011**, *21*, 4712**–**4718.
33) Dynamics and Transient Absorption Spectral Signatures of the Single-Wall Carbon Nanotube Electronically Excited Triplet State, J. Park, P. Deria, and M. J. Therien, *J. Am. Chem. Soc.* **2011**, *133*, 17156–17159.
34) Near IR Nonlinear Absorption of an Organic Supermolecule, S.-H. Chi, A. Rosenberg, A. Nayak, T. V. Duncan, M. J. Therien, J. J. Butler, S. R. Montgomery, G. Beadie, R. G. S. Pong, J. S. Shirk, and S. R. Flom, *Opt. Mater. Express* **2011**, *1*, 1383-1392.
35) Composite Electronic Materials Based on Poly(3,4-propylenedioxythiophene) and Highly Charged Poly(aryleneethynylene)-Wrapped Carbon Nanotubes for Supercapacitors, M. R. Rosario-Canales, P. Deria, M. J. Therien, and J. J. Santiago-Avilés, *ACS Appl. Mater. Interfaces* **2012**, *4*, 102-109.
36) Acentric 2-D Ensembles of D-br-A Electron-Transfer Chromophores via Vectorial Orientation within Amphiphilic n-Helix Bundle Peptides for Photovoltaic Device Applications, J. Koo, J. Park, A. Tronin, R.

Zhang, V. Krishnan, J. Strzalka, I. Kuzmenko, H. C. Fry, M. J. Therien, and J. K. Blasie, *Langmuir* **2012**, *28*, 3227–3238.

37) Design of Coupled Porphyrin Chromophores with Unusually Large Hyperpolarizability, N. Jiang, G. Zuber, S. Keinan, A. Nayak, W. Yang, M. J. Therien, and D. N. Beratan, *J. Phys. Chem. C*. **2012**, *116*, 9724–9733.
38) Electronic Transport in Porphyrin Supermolecule-Gold Nanoparticle Assemblies, D. Conklin, S. Nanayakkara, T.-H. Park, M. F. Lagadec, J. T. Stetcher, M. J. Therien, and D. A. Bonnell, *Nano Lett*. **2012**, *12*, 2414**–**2419.
39) Quasi-Ohmic Single Molecule Charge Transport through Highly Conjugated *meso*-to-*meso* Ethyne-Bridged Porphyrin Wires, Z. Li, T.-H. Park, J. Rawson, M. J. Therien, and E. Borguet, *Nano Lett*. **2012**, *12*, 2722–2727.
40) Enhanced Dispersion of CdSe/MEH-CN-PPV Hybrid Nanocomposites by in situ Polymerization using AEM as Photopolymerizable Precursor, Y. Park, J. Park, M. J. Therien, and A. D. Stiff-Roberts, *Colloid Polym. Sci*. **2012**, *290*, 1501**–**1509.
41) Effect of Solvent Polarity and Electrophilicity on Quantum Yields and Solvatochromic Shifts of Single-Walled Carbon Nanotube Photoluminescence, B. A. Larsen, P. Deria, J. M. Holt, I. N. Stanton, M. J. Heben, M. J. Therien, and J. L. Blackburn, *J. Am. Chem. Soc*. **2012**, *134*, 12485**–**12491.
42) Exploiting Plasmon Induced Hot Electrons in Molecular Electronic Devices, D. Conklin, S. Nanayakkara, T.-H. Park, M. F. Lagadec, J. T. Stetcher, X. Chen, M. J. Therien, and D. A. Bonnell, *ACS Nano*, **2013**, *7*, 4479**–**4486.
43) Raman Spectroscopic Investigation of Individual Single-Walled Carbon Nanotubes Helically Wrapped by Ionic, Semiconducting Polymers, S. Bonhommeau, P. Deria, M. G. Glesner, D. Talaga, S. Najjar, C. Belin, L. Auneau, S. Trainini, M. J. Therien, and V. Rodriguez, *J. Phys. Chem. C*. **2013**, *117*, 14840**–**14849.
44) Origins of the Helical Wrapping of Phenylene-Ethynylene Polymers about Single-Walled Carbon Nanotubes, C. D. Von Bargen, C. M. MacDermaid, O.-S. Lee, P. Deria, M. J. Therien, and J. G. Saven, *J. Phys. Chem. B*. **2013**, *117*, 12953–12965.
45) The Evolution of Spin Distribution in the Photoexcited Triplet State of Ethyne-Elaborated Porphyrins, P. J. Angiolillo, J. Rawson, P. R. Frail, and M. J. Therien, *Chem. Commun*. **2013**, *49*, 9722-9724.
46) Computational De Novo Design and Characterization of a Protein that Selectively Binds a Highly Hyperpolarizable Abiological Chromophore, H. C. Fry, A. Lehmann, L. E. Sinks, I. Asselberghs, A. Tronin, V. Krishnan, J. K. Blasie, K. Clays, W. F. DeGrado, J. G. Saven, and M. J. Therien, *J. Am. Chem. Soc*. **2013**, *135*, 13914**–**13926.
47) Ionic Self-Assembly Provides Dense Arrays of Individualized, Aligned Single Walled Carbon Nanotubes, J.-H. Olivier, P. Deria, J. Park, A. Kumbhar, M. Andrian-Albescu, and M. J. Therien, *Angew. Chemie*. **2013**, *52*, 13080-13085.
48) Single-Handed Helical Wrapping of Single-Walled Carbon Nanotubes by Chiral, Ionic, Semiconducting Polymers, P. Deria, C. D. Von Bargen, J.-H. Olivier, A. S. Kumbhar, J. G. Saven, and M. J. Therien, *J. Am. Chem. Soc*. **2013**, *135*, 16220**–**16234.
49) Fluence-Dependent Singlet Exciton Dynamics in Length-Sorted Chirality-Enriched Single-Wall Carbon Nanotubes, J. Park, P. Deria, J.-H. Olivier, and M. J. Therien, *Nano Lett*. **2013**, *13*, DOI: 10.1021/nl403511s.
50) One-Pot Solvothermal Synthesis of Highly Emissive, Sodium-codoped, LaF_3 and $BaLaF_5$ Core-Shell Upconverting Nanocrystals, J. T. Stecher, A. B. Rohlfing, and M. J. Therien, *Nanomaterials* **2013**, DOI:10.3390/nano4010069.
51) The Biochemistry and Theory of Proton Coupled Electron Transfer, A. Migliore, N. F. Polizzi, M. J. Therien, and D. N. Beratan, *Chem. Rev*. Submitted.
52) A Fiber-Optic Radiation Detector Based on Europium-Doped Yttrium Oxide Nanocrystals that Provides a Linear Emissive Response to X-ray Radiation Exposure, I. N. Stanton, M. D. Belley, G. Nguyen, A. Rodrigues, Y. Li, D. G. Kirsch, T. T. Yoshizumi, and M. J. Therien, *Anal. Chem*. Submitted.

BIOGRAPHICAL SKETCH

Provide the following information for the Senior/key personnel and other significant contributors in the order listed on Form Page 2.
Follow this format for each person.

NAME Spector, Neil L.	POSITION TITLE Associate Professor of Medicine (Oncology)
eRA COMMONS USER NAME (credential, e.g., agency login) Spect002	

EDUCATION/TRAINING *(Begin with baccalaureate or other initial professional education, such as nursing, include postdoctoral training and residency training if applicable.)*

INSTITUTION AND LOCATION	DEGREE *(if applicable)*	MM/YY	FIELD OF STUDY
University of North Carolina, Chapel Hill	B.S.	5/1978	Pre-Med
New Jersey Medical School UMDNJ	MD.	6/1982	Medicine
Parkland Memorial Hospital, UT-Southwestern		6/1982-6/1986	Internship & Residency

A. Personal Statement. I have a long standing interest in elucidating mechanisms involved in tumorigenesis and the development of molecule to target these pathways. My group has performed extensive work in targeting HER2 and other EGFR family members and has a successful track record in translating research from the bench to the clinic. My group led the translational research program that was instrumental in the development of lapatinib, the first small molecule inhibitor of the EGFR and HER2 tyrosine kinases approved for the treatment of women with HER2+ breast cancer. Our work led to insight into the molecular signatures of tumors that were more likely to respond to lapatinib, and conversely those that were likely to be resistant. We successfully developed the first reported models of acquired resistance to HER2 TKIs that mimic the clinical setting. Using these models, we showed that successful inhibition of PI3K-Akt signaling in lapatinib-treated HER2+ breast cancer cells led to de-repression of the FOXO3a transcription factor with consequential activation of estrogen receptor (ER) signaling. Co-treatment with anti-estrogens and lapatinib could abrogate lapatinib resistance in pre-clinical models, which provided the scientific basis for a clinical development plan combining an aromatase inhibitor with lapatinib, a combination approved by the FDA as a first-line therapy for the treatment of advanced stage ER+/HER2+ breast cancers. In addition, we have identified a number of other molecular mechanisms of therapeutic resistance to HER2 targeted therapies. Since coming to Duke in 2006, I have been eager to continue my interests in drug development as the co-leader of the Developmental Therapeutics Program (DTP) in the Duke Cancer Institute. I am on a number of multi-investigator grants specifically designed to take novel therapeutics discovered at Duke and bring them into the clinic. In my leadership role in the DTP, I have sought to create an environment that will facilitate the critical partnerships necessary to translate discoveries made by Duke investigators, into the clinic.

B. B. Positions and Honors

1986-1988 **Clinical Hematology and Medical Oncology,** Massachusetts General Hospital, Harvard Medical School, Boston, MA (Fellowship)

1988-1989	Research Fellow in Tumor Immunology and Bone Marrow Transplantation, Dana-Farber Cancer Institute, Harvard Medical School, Boston, MA (Fellowship)
1989-1993	Instructor in Medicine, Dana-Farber Cancer Institute, Division of Tumor Immunology, Harvard Medical School
1993-1998	Assistant Professor of Medicine, Division of Hematology/Oncology and Department of Molecular Biology/Biochemistry, University of Miami School of Medicine, Miami, FL
1998-1999	Senior Clinical Research Physician, Head of Experimental Medicine Oncology Laboratory, GlaxoWellcome, Research Triangle Park, NC
1998-2000	Therapeutic Area Scientist VII, Head of Experimental Medicine Oncology, GlaxoWellcome
2001-2006	Head of Exploratory Medical Sciences-Oncology, Discovery Medicine, GlaxoSmithKline
2000-2006	Adjunct Associate Professor of Medicine, Division of Hematology/Medical Oncology, Lineberger Comprehensive Cancer Center, University of North Carolina-Chapel Hill, Chapel Hill, NC
2006-Present	Co-Director Development Therapeutics Program, Associate Director, Clinical Research Breast Cancer Program, Duke Center Institute, Associate Professor of Medicine, Division of Medical Oncology, Duke University School of Medicine, Durham, NC
2007-Present	Secondary Appointment (Associate Professor) in the Department of Pharmacology/Cancer Biology, Duke University School of Medicine, Durham, NC

C. Selected Peer-reviewed Publications

1. Kurokawa M, Kim J, Geradts J, Mastuura K, Liu L, Xia W, Ribar TJ, Dewhirst MW, Kim W-J, Lucas JE, Wang S, Spector NL, & Kornbluth S. "A novel network of MDM2 and HUWE1 substrates controlling apoptosis independently of p53." *Sci Signal*. 2013 May 7;6(274):ra32. doi: 10.1126/scisignal.2003741..
2. Xia W, Petricoin III EF, Zhao S, Liu L, Osada T, Cheng Q, Wulfkuhle JD, Yang X, Gallagher RI, Clay T, Bacus S, Lyerly HK, & Spector NL. "An heregulin EGFR-HER3 signaling axis can mediate acquired resistance in HER2+ breast cancer models." *Breast Cancer Res* (in press).
3. Xia W, Liu Z, Zong R, Liu L, Zhao S, Bacus S, Mao Y, He J, Wulfkuhle J, Petricoin III E, Osada T, Yang X, Hartman Z, Clay T, Blackwell K, Lyerly K, & Spector NL. "Truncated ErbB2 expressed in tumor cell nuclei contributes to acquired therapeutic resistance to ErbB2 kinase inhibitors". *Mol Cancer Ther*.2011;10:1367-1374.
4. Il'yasova D, Siamakpour-Reihani S, Akushevich I, Akushevich L, Spector NL, & Schildkraut J. "What can we learn from the age-and race/ethnicity-specific rates of inflammatory breast cancer?" *Breast Cancer Res Treat*. 2011 Nov:130(2): 691-697.
5. Xia W, Bacus S, Husain I, Liu L, Zhao S, Liu Z, Moseley MA III, Thompson JW, Chen FL, Koch KM, & Spector NL. "Resistance to ErbB2 Tyrosine Kinase Inhibitors in Breast Cancer Is Mediated by Calcium-Dependent Activation of RelA". *Mol Cancer Ther*. 2010; 9: 292-299.
6. Boussen H, Cristofanilli M, Zaks T, DeSilvio M, Salazar V, & Spector NL. "Phase II Study to Evaluate the Efficacy and Safety of Neoadjuvant Lapatinib in Combination With Paclitaxel in Patients With Newly Diagnosed Inflammatory Breast Cancer" *J. Clin. Oncol*., 2010; 28: 3248-3255. Epub 2010 Jun 7.
7. Kaufman B, Trudeau M, Awada A, Blackwell K, Bachelot T, Salazar V, DeSilvio M, Westlund R, Zaks T, Spector N, & Johnston S. "Lapatinib monotherapy in patients with HER2-overexpressing relapsed or refractory inflammatory breast cancer: final results and survival of the expanded HER2+ cohort in EGF103009, a phase II study." *Lancet Oncol*., 2009 Jun;10(6):581-8. Epub 2009 Apr 24.
8. Johnston S, Trudeau M, Kaufman B, Boussen H, Blackwell K, Lorusso P, Lombardi DP, Ahmed SB, Citrin DL, DeSilvio ML, Harris J, Salazar V, Zaks TZ, & Spector NL. "Targeting HER2 in advanced inflammatory breast cancer with lapatinib monotherapy: A phase II study with biomarker profiles that predict for response" *J. Clin. Oncol*. 2008; 26: 1066-1072.

9. Spector NL, Yarden Y, Smith B, Lyass L, Trusk P, Pry K, Hill JE, Xia W, Seger R, & Bacus SS. "Activation of AMPK regulated metabolic stress response by a small molecule HER2/EGFR tyrosine kinase inhibitor protects cardiac myocytes from apoptosis" *Proc. Natl. Acad. Sci USA* 2007; 104: 10607-10612.
10. Xia W, Husain I, Leihua L, Bacus S, Saini S, Spohn J, Pry K, Westlund R, Stein S, & Spector NL. "Lapatinib anti-tumor activity is not dependent upon PTEN in ErbB2-overexpressing breast cancers" *Cancer Res*., 2007; 67: 1170-1175.
11. Xia W, Bacus S, Hegde P, Husain I, Strum J, Liu L, Paulozzo G, Trusk P, Lyass L, & Spector NL. "A model of acquired autoresistance to ErbB2 tyrosine kinase inhibitors and a therapeutic strategy to prevent its onset in breast cancer" *Proc. Natl. Acad. Sci. USA* 2006; 103: 7795-7800.
12. Xia W, Bisi J, Strum J, Liu L, Carrick K, Graham KL, Hardwicke MA, Treece AL, Bacus S, & Spector NL. "Regulation of survivin by ErbB2 signaling: Therapeutic implications for ErbB2-overexpressing breast cancers" *Cancer Res*., 2006; 66: 1640-1647.
13. Burris H, Dees C, Hurwitz H, Dowlati A, Blackwell K, Marcom K, Overmoyer B, Smith D, Koch K, Stead A, Mangum S, Harris J, & Spector NL. "A phase I safety, pharmacokinetic, and clinical activity study of lapatinib (GW572016), a reversible inhibitor of ErbB1 and ErbB2 tyrosine kinases in heavily pre-treated patients with metastatic carcinomas" *J. Clin. Oncol,* 2005; 23: 5305-5313.
14. Spector NL, Xia W, Burris HA, Hurwitz H, E. Claire Dees, Dowlati A, O'Neil B, Overmoyer B, Liu L, Marcom K, Blackwell K, Smith DA, Koch K, Mangum SG, Stead A, Greco FA, Harris J, & Bacus SS. "A Study of the biological effects of GW572016, a reversible inhibitor of EGFR (ErbB1) and ErbB2 tyrosine kinases, on tumor growth and survival pathways in patients with advanced malignancies" *J. Clin. Oncol*., 2005; 23: 1-11.
15. Xia W, Gerard C, Lui L, Baudson N, Ory T, & Spector NL. "Lapatinib (GW572016), a small molecule inhibitor of ErbB1 and ErbB2 tyrosine kinases synergizes with anti-ErbB2 antibodies to inhibit mediators of tumor cell survival and induce apoptosis in ErbB2 overexpressing breast cancer cells" *Oncogene* 2005; 24: 6213-6221.
16. Xia W, Liu L-H, Ho P, & Spector NL. "Truncated ErbB2 receptor (p95ErbB2) is regulated by heregulin through heterodimer formation with ErbB3, yet remains sensitive to the dual EGFR/ErbB2 kinase inhibitor GW572016" *Oncogene* 2004; 23: 646-653.